Modeling Human Visuomotor Adaptation with a Disturbance Observer Framework

Gaurav Sharma [1,2], Bernard Marius 't Hart [1], Jean-Jacques Orban de Xivry [3,4], Denise Y.P. Henriques [1,2,5], Mireille E. Broucke [6*],

1 Centre for Vision Research, York University, Toronto, ON, Canada
2 Department of Psychology, York University, Toronto, ON, Canada
3 Department of Movement Sciences, KU Leuven, Belgium
4 Leuven Brain Institute, KU Leuven, Belgium
5 School of Kinesiology and Health Science, York University, Toronto, ON, Canada
6 Department of Electrical and Computer Engineering, University of Toronto, Toronto, ON, Canada

*broucke@control.utoronto.ca

Abstract

Visuomotor adaptation studies have revealed a range of behaviors, including nonlinear saturation effects, instruction-dependent differences in performance, and distinct explicit and implicit components of adaptation. However, existing computational models have struggled to account for the full breadth of these findings. In this paper, we aim to address this gap by (1) designing a set of experiments to investigate the role of nonlinear saturation under different instructional contexts, and (2) introducing an abstract discrete-time model that captures plausible neural computations underlying the observed behaviors. The model draws on recent advances in control theory and is informed by prior work on oculomotor adaptation and cerebellar function, particularly within the floccular complex.

Author summary

A central research challenge in the field of motor learning is to disentangle the components of motor learning [1–8]. The main hypothesis explored in this paper is that visuomotor rotation experiments in which participants are given distinct instructions to either move the hand or the cursor to the target offer a platform to explore two components of motor learning arising from different computations and possibly different brain regions. The two computations correspond to a *disturbance observer* whose role is to detect and then eliminate environmental perturbations and a *feedforward system* whose role is to learn from the disturbance observer to improve feedforward motor commands.

1 Introduction

Motor control has long served as a fertile domain for applying concepts from control theory. Four core tools have been particularly influential: feedback control, optimal control theory, Kalman filtering, and internal models — especially forward and inverse models. Feedback control plays a foundational role because it renders the closed-loop system to be robust to transient disturbances: it is unparalleled in terms of low complexity, speed of response, and effectiveness. Optimal control theory complements feedback control by formalizing goal-directed movement generation [9], identifying desirable trajectories and control strategies under specified cost functions — for example, minimum metabolic cost reaching movements [10].

The Kalman filter, a prototypical forward model, fuses motor commands with noisy sensory data to estimate latent states of the system. These estimates are critical for prediction, online correction, and motor learning [11]. Inverse models, introduced in motor control contexts in [12, 13], compute open-loop control commands based on the system's current state and desired goals. Forward models — also known as observers in control theory — predict future system states and have been widely studied in biological motor systems [3, 14–20]. Forward models have also been considered in the context of estimating environmental disturbances [21]. Adaptive forward models account for discrepancies between predicted and actual system dynamics, such as model parameter mismatches.

Despite a rich landscape of methodologies to understand motor control, visuomotor adaptation presents a distinct challenge: here, the perturbation lies not in the system, but in the sensory error signal itself — typically in the visual feedback of movement. The adaptation process must therefore compensate for altered sensory consequences rather than changes in the body or task mechanics. This framing naturally aligns with the use of adaptive filters, which are designed to detect and remove distortions in incoming signals [22–24]. More specifically, it connects with *regulator theory*, which addresses the elimination of persistent disturbances from error signals. Central to this theory is the **internal model principle**, which states that "every good controller must contain an internal model of all (unmeasurable) reference and disturbance signals impinging on a control loop" [25, 26]. In this sense, visuomotor adaptation can be interpreted as the implementation of a biological regulator that aims to drive steady state sensory error to zero.

In this work, we propose a discrete-time behavioral state-space model of visuomotor adaptation designed to account for both the experimental findings reported here and phenomena observed in prior studies. The model architecture (Fig 1) consists of three core components: (i) a fast-reacting error feedback process, which aligns with single-trial learning effects (not shown in the figure); (ii) a disturbance observer, which estimates persistent perturbations in the visual error signal and drives their asymptotic elimination; and (iii) a slower feedforward learning system that gradually updates internal control commands through a process of learning transfer from the disturbance observer.

The disturbance observer and feedforward system are dynamically coupled; however, the dominant mode of interaction is a cascade architecture in which the disturbance observer continuously influences the feedforward learner. Additionally, the model includes the possibility of a phase switch, representing a transition between the actively expressed computational module or strategy, consistent with observations of context-dependent changes in behavior.

The disturbance observer functions as a specialized internal model that isolates and

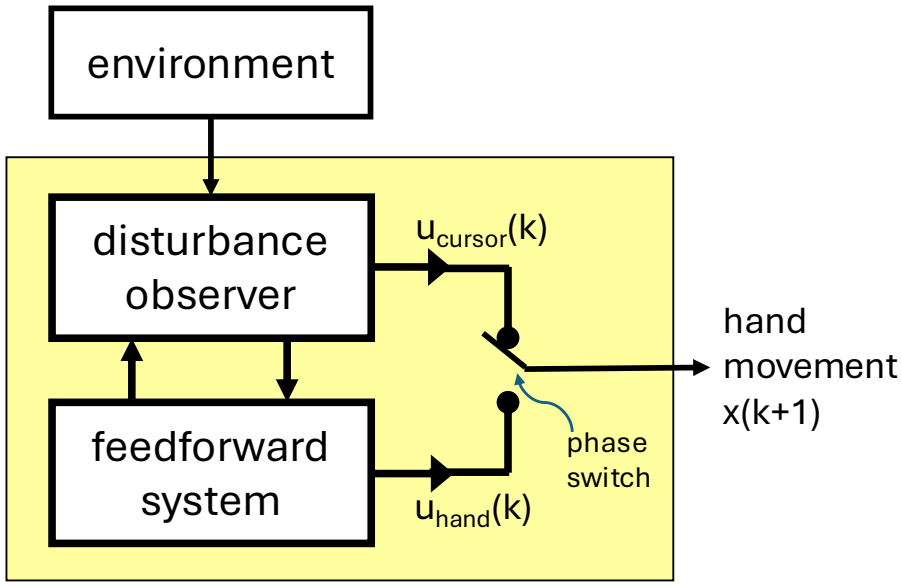

Fig 1. Block diagram of the proposed visuomotor model.

compensates for persistent exogenous disturbances affecting the sensory error signal. While related to observer constructs in control theory, disturbance observers have not, to our knowledge, been systematically applied within sensorimotor modeling. A central aim of this paper is to demonstrate their utility for explaining key features of visuomotor adaptation.

The second major component, the feedforward system, underlies the ability to execute accurate reaching movements in the absence of visual feedback or under instructions to "move the hand to the target." It updates internal motor commands based on sustained discrepancies identified by the disturbance observer — effectively learning from evidence of persistent miscalibration. This process unfolds over a medium to long timescale and supports adaptation beyond immediate error-based corrections. The inclusion of both the disturbance observer (driving computations when a cursor is visible and the participant is instructed to move the cursor to the target) and a feedforward system (driving computations when there is no cursor or the instructions are to move the hand to the target) means that the DO model can also account for so-called *phase switches*, switches in computational streams in the brain, a capability concurring with experimental studies on rapid switching between motor plans [27]. Phase switches have been observed when trials alternate between a series of reaches with a misaligned cursor and subsequent no-visual feedback trials [28]. While this transition has often been attributed to the removal of an explicit strategy, recent results [29] suggest that it cannot be fully explained in this way. Our current work shows that this behavior can instead be captured within a computational framework.

A particular challenge in modeling visuomotor adaptation lies in capturing the behavioral consequences of varying participant instructions and the nonlinear saturation observed in paradigms such as error clamp experiments. To address this, we designed a visuomotor reaching task that introduces a novel manipulation: a hand angle-gain parameter, denoted by α, which scales the angular displacement of the hand relative to the target, independently of the standard visuomotor rotation applied to the visual cursor. See Fig 2.

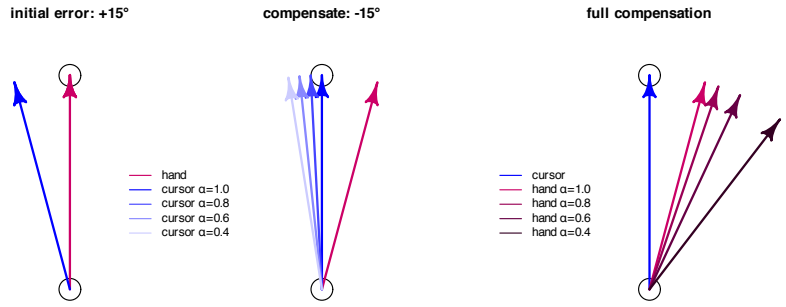

Fig 2. Effect of the hand angle-gain (α) on the cursor direction. The left figure shows the initial observed visual error due to a perturbation of $+15°$. The middle figure shows the compensation of the hand angle by $-15°$ to overcome the initially observed visual error of magnitude $+15°$ with $\alpha = 1.0$. The shaded blue arrows show the effect on the cursor direction for $\alpha \in \{0.8, 0.6, 0.4\}$ with lighter blue for smaller α. We see that as α is decreased, the cursor direction progressively approaches a constant value of $115°$. The right figure depicts the required compensation of the hand angle to place the cursor on the target for $\alpha \in \{1.0, 0.8, 0.6, 0.4\}$.

This gain-based manipulation allows us to implement error clamp conditions in a graded, parametric manner. Specifically, $\alpha = 0$ corresponds to a full error clamp, while $\alpha = 1$ corresponds to standard adaptation conditions. By systematically varying α between 0 and 1 — assigning a fixed gain per experiment — we observe the progressive emergence of saturation effects. This graded approach offers a principled way to study and model nonlinear learning behavior. To our knowledge, this experimental method has not been previously employed; prior work has focused primarily on error augmentation paradigms [30, 31]. Our findings suggest that the error clamp should not be treated as a singular or exceptional case, but rather as an integral part of the behavioral response continuum — one that any comprehensive model of visuomotor adaptation must account for.

2 Materials and Methods

Participants. Experiments 1 and 2 involved 29 participants (males = 15, females = 14, age range = $18 - 32$, age (mean $\pm$ standard deviation) = 21.69 ± 3.41 years). Experiments 3 and 4 involved 51 participants (males = 20, females = 31, age range = $18 - 38$, age (mean $\pm$ standard deviation) = 21.7 ± 4.73 years). All the participants self-reported to be right-handed or left-handed, and having normal or corrected-to-normal vision. Also, prior to the data collection, all participants signed and were informed with a written consent form. This study was approved by York University's Human Participants Review Committee and all procedures were performed in accordance with institutional and international guidelines.

Experimental Setup. The setup is illustrated in Fig 3 and consisted of a downward-facing LCD screen (60 Hz, 20 in, 1680×1050, Dell E2009Wt), a tablet and stylus (Wacom Intuos Pro PTH860) to record the hand position, and an upward facing mirror placed in between the tablet and screen. In-house software was created to design

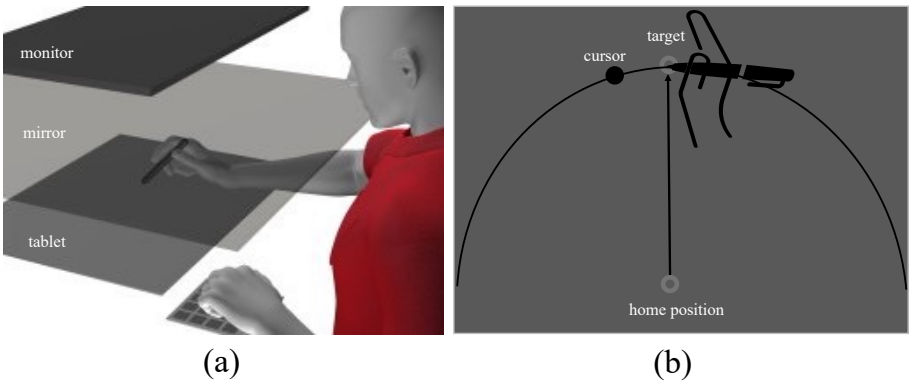

Fig 3. (a) Experimental apparatus for presenting a visuomotor reaching task. (b) Representation of a trial with visual feedback.

and conduct visuomotor reach experiments (https://github.com/thartbm/PyVMEC2). Visual stimuli were presented via a downward-facing LCD screen positioned above an upward-facing mirror, such that the reflected image appeared aligned with the horizontal plane as the participants' hand. Participants were seated in a height-adjustable chair, allowing them to comfortably execute out-and-back reaching movements on the tablet by using a stylus held in their dominant hand. A black cloth was placed over the shoulder to occlude vision of the arm.

Visuomotor Reaching Task. Participants made outward reaches toward a target by smoothly gliding the stylus on the tablet starting from a home position, as shown in Fig 3. Each trial began at a central home position, displayed as an open gray circle (radius 0.5 cm) on the screen. The reach target, also an open gray circle of the same size, appeared 8 cm from the home position, generally in the forward direction. The target appeared when the stylus entered the home position. Participants were instructed to move toward the target at a comfortable pace — neither too fast nor too slow — and to avoid resting their wrist or elbow on the tablet or surrounding surface during the reach.

Two types of trials were included, based on task instructions. In **Learn** trials, participants were instructed to move the *cursor* to the target, promoting adaptation to visuomotor errors. In **Ignore** trials, they were instructed to move their *unseen hand* to the target location, regardless of cursor position, thus minimizing reliance on visual feedback. Both trial types were performed under continuous cursor feedback. The first two experiments also included **No cursor** trials in which a cursor was not presented and participants were instructed to move the unseen hand directly to the target. The second two experiments included **Washout** trials with veridical cursor feedback and instructions to move the cursor to the target.

In trials with visual cursor feedback, a black cursor (radius 0.5 cm) continuously represented the stylus position, allowing participants to track their unseen hand. In no cursor trials, the cursor was not visible during the reach. To encourage consistent movement speeds, auditory feedback was provided based on the movement duration. Outward movements lasting between 0.2s and 0.4s triggered a pleasant tone, while movements that were too fast, too slow, or initiated before target onset triggered an unpleasant tone. At the end of each trial, participants were instructed to return their hand to the home position to initiate the next trial. As the hand was not visible, a physical stencil was used to guide the hand back to the start location reliably.

Hand Angle-Gain. Next we explain the rule used to determine the cursor direction for Learn and Ignore trials. Let d denote the perturbation (rotation in degrees), $r(k)$ the direction of a target on the k-th trial, and $x(k)$ the hand angle on the k-th trial. We introduce a parameter α called the *hand angle-gain* that takes one of four values in the first two experiments: $\alpha \in \{0.4, 0.6, 0.8, 1.0\}$. The cursor was placed at the following angle

$$y(k) = r(k) + \alpha(x(k) - r(k)) + d\,. \tag{1}$$

This rule ensured that the cursor was displayed at an angle offset by the rotation d, while the hand's contribution to that offset was scaled by α. When $\alpha = 1.0$, the cursor directly reflects the rotated hand angle — standard visuomotor rotation. As α decreases toward 0, the cursor movement is increasingly clamped to the target direction plus the perturbation, effectively simulating error clamp conditions.

Fig 2 illustrates the behavior of the cursor direction for a target positioned straight ahead at $r = 90°$ and a perturbation $d = 15°$. In the left panel, the participant initially aims for $x(k) = 90°$, causing the cursor to appear at $y(k) = r + d = 105°$. In the middle panel, the participant compensates for the initial error by adjusting their reach in the direction opposite to the perturbation. According to (1), the hand angle is scaled by parameter α, which moves the red arrow closer to the target. This adjusted hand angle is then rotated by $d = 15°$ to produce the cursor angle, shown as graded blue arrows, each corresponding to a different α value. As α decreases, the hand angle is progressively shifted towards the target angle, and the cursor angle moves closer to the original cursor angle shown in the left panel. When $\alpha = 0$, the hand angle is fully suppressed (multiplied by zero) and rotated by 15°, resulting in a constant cursor angle at $y = 105°$, a condition known as the error clamp [32]. Conversely, when $\alpha = 1$, the participant experiences a standard learning trial without any scaling of the hand movement. The right panel of Fig 2 illustrates the hand angle required to fully compensate for the perturbation, effectively eliminating the observed error and aligning the cursor with the target.

Experimental Structure. The experimental study included four experiments. In Experiments 1 and 2, each participant completed the visuomotor reaching task across two experimental sessions, separated by a minimum of three days. The experimental structure was identical across sessions to assess within-participant consistency and to ensure adequate data for analysis. In each session, participants performed two distinct experiments (1 and 2). In Experiments 3 and 4, participants completed only one type of experiment in one session only.

As illustrated in Fig 4, Experiments 1 and 2 were organized into four sequential cycles, indicated by vertical dashed lines. Each cycle consisted of three phases: a baseline phase, a rotation phase, and a no cursor phase. A brief one-minute break was provided between cycles in both experiments. During this time, on-screen instructions were presented to remind participants of the upcoming task requirements. Experiments 3 and 4 consisted of only one cycle with three phases.

- **Experiment 1** (**Ignore-N Experiment**) consisted of four cycles, each with three trial phases (Fig 4). Each cycle began with a baseline phase of 40 trials in which the cursor accurately represented the stylus position (i.e., veridical feedback, no rotation). This was followed by a phase of **Ignore** trials, in which participants were instructed to move their *unseen hand* to the target while a visuomotor rotation (perturbation) was applied to the cursor. In addition to the perturbation, an angular gain factor — referred to as the *hand angle-gain* α — was applied to the hand trajectory to manipulate the relationship between the hand angle and

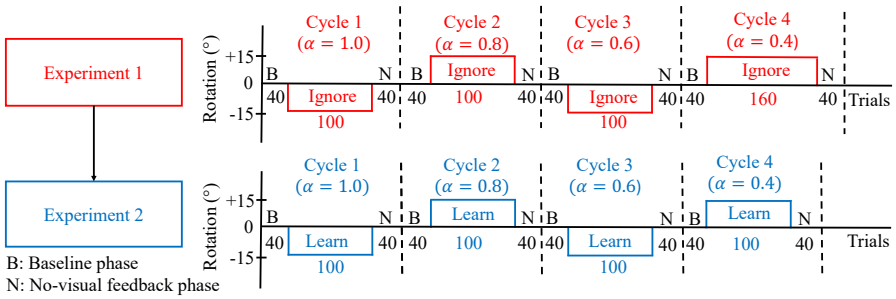

Fig 4. Trial structure for Experiments 1 and 2, with Experiment 1 performed first. In Experiment 1 (Ignore-N) participants were instructed to move their invisible hand to the target while ignoring the cursor. The experiment was conducted in four cycles, denoted cycle 1 to cycle 4. Each cycle began with a baseline phase (B) of 40 trials with no rotation and a hand angle-gain (α) = 1.0, followed by a rotation phase of Ignore trials with ± 15° rotation. Each cycle ended with a no cursor phase (N) of 40 trials with no rotation and $\alpha = 1.0$. In the Ignore trials of each cycle, participants experienced one of four different values of α: 1.0, 0.8, 0.6, and 0.4. In Experiment 2 (Learn-N) participants were instructed to move the cursor to the target. The experiment was also conducted in four cycles. Each cycle began with a baseline phase (B) of 40 trials with no rotation and $\alpha = 1.0$, followed by a rotation phase of Learn trials with ± 15° rotation. Each cycle again ended with a no cursor phase (N) of 40 trials with no rotation and $\alpha = 1.0$. In the Learn trials of each cycle, participants experienced one of four different values of α: 1.0, 0.8, 0.6, and 0.4. There was a one-minute break in between each cycle of these experiments, and during that time, particular instructions were displayed on the screen for the upcoming trials.

the resulting cursor angle. Further details about the implementation and rationale for α are provided below. Each cycle concluded with a phase of 40 **No cursor** trials, during which the cursor was not visible throughout the reach. Targets in Experiment 1 were presented at one of five angular locations: 80°, 85°, 90°, 95°, or 100°, relative to the center.

The Ignore phase of Experiment 1 introduced both a ±15° visuomotor rotation as well as a hand angle-gain α. To minimize carryover effects in this within-subject design, the sign of the rotation alternated across cycles (e.g., +15°, −15°, +15°, −15°). Additionally, across the four cycles, α took values of 1.0, 0.8, 0.6, or 0.4, allowing a progressive attenuation of the effect of the hand movement on the cursor placement — approaching an error clamp as α is decreased (see Fig 2). The hand angle-gain α was always set to 1.0 during the baseline phase, and it is not relevant in the no cursor phase.

The number of Ignore trials within a cycle depended on α. For $\alpha = 1.0$, 0.8, or 0.6, the Ignore phase contained 100 trials. For $\alpha = 0.4$, the number of Ignore trials was increased to 160 to allow for sufficient data under near-clamp conditions.

- **Experiment 2** (**Learn-N Experiment**) followed a similar structure as Experiment 1, with each cycle beginning with 40 baseline trials and concluding with 40 no cursor trials. The central phase of each cycle consisted of 100 **Learn** trials, in which participants were instructed to move the *cursor* to the target. During the Learn phase, both a rotation and a hand angle-gain were applied to the cursor, following the same pattern as for Experiment 1. Targets in Experiment 2 were presented at one of five angular locations: 80°, 85°, 90°, 95°, or 100°,

relative to the center.

- **Experiment 3** (**Ignore-W Experiment**) included only one cycle with three phases. The experiment began with 40 baseline trials and concluding with 40 **Washout** trials with veridical cursor feedback. The central phase of this experiment consisted of 120 Ignore trials. During the Ignore trials, the perturbation was either 25° CW or CCW, and the value of α was one of $\{0.5, 0.75, 1.0\}$. Five targets were placed at every 5° from 140° to 160° for a CCW perturbation; while five targets were placed at every 5° from 20° to 40° for a CW perturbation. Each participant experienced either a CW or CCW rotation, but not both, and only one value of α within the session.

- **Experiment 4** (**Learn-W Experiment**) had the same structure as Experiment 3, but participants performed Learn trials instead of Ignore trials.

Data Analysis: The performance of each participant was evaluated by measuring the angular reach deviation for each trial. The angular deviation was computed as the angle between a line through the target and a line through the point of maximum velocity of the hand. Baseline biases for each participant were calculated by using the average angular reach deviation over the last 20 trials of the baseline phase. The angular reach deviation of each trial was then corrected based on each participant's baseline biases. Finally, the mean reach deviation was computed over all participants using the bias-corrected data. All raw and summary data are publicly available: https://osf.io/gjb5r/.

In the experiments, the target was placed at one of five randomized locations; for instance, between 80° and 100° in Experiments 1 and 2. However, for the simulations, we normalize the data to treat the target as if it were always at 90°, representing a single direction within the adaptation field. For the experimental data from other studies, hand angles were averaged over targets and over participants. A bias correction using the baseline phase of the averaged participant data was only applied to the data from [33].

3 Disturbance Observer (DO) Model

We present a nonlinear state-space model of the visuomotor reach experiment called the **Disturbance Observer** (DO) Model. All angular quantities in the DO model are in units of degrees, with 90° representing the straight ahead direction - defined as a horizontal line through the participant's sagittal plane while seated. The index k denotes the trial number; $x(k)$ denotes the hand angle on the k-th trial; and $r(k)$ denotes the angular position of the target for the k-th trial. Index j is the j-th trial when a cursor is visible, $d(j)$ denotes the perturbation for the j-th trial, and $y(j)$ denotes the cursor angle on the j-th trial. For each trial, the participant is instructed either to move the hand to the target or move the cursor to the target. All states as well as indices k and j are initialized to zero (states can be initialized to any value set by the user).

- If a cursor is displayed on the k-th trial, perform the following updates:

$$j = j + 1 \tag{2a}$$
$$y(j) = r(k) + \alpha(x(k) – r(k)) + d(j) \tag{2b}$$
$$e(j) = r(k) - y(j) \tag{2c}$$
$$u_s(j) = Ke(j) \tag{2d}$$
$$\hat{w}(j) = w_0(j) + Ge(j) \tag{2e}$$
$$u_{im}(j) = \psi(j)\hat{w}(j) \tag{2f}$$
$$u(k) = \begin{cases} r(k) + u_f(k) + u_s(j) + u_{im}(j) & \text{Learn} \\ r(k) + u_f(k) + x_f(k) & \text{Ignore} \end{cases} \tag{2g}$$
$$w_0(j+1) = Fw_0(j) + FGe(j) + G(u(k) - r(k) - u_f(k)) \tag{2h}$$
$$x_f(k+1) = A_f x_f(k) + (1 - A_f)L(j)u_{im}(j) \tag{2i}$$
$$u_f(k+1) = u_f(k) + L_f x_f(k) \tag{2j}$$
$$x(k+1) = u(k) \tag{2k}$$

- If no cursor is displayed on the k-th trial, perform the following updates:

$$u(k) = \begin{cases} r(k) + u_f(k) + u_s(j) + u_{im}(j) & \text{Learn} \\ r(k) + u_f(k) + x_f(k) & \text{Ignore} \end{cases} \tag{2l}$$
$$x_f(k+1) = A_{fn} x_f(k) \tag{2m}$$
$$u_f(k+1) = u_f(k) \tag{2n}$$
$$x(k+1) = u(k) \tag{2o}$$

If we select $\psi(j) = \psi_\circ$ and $L(j) = L_\circ$ to be constants, then the DO model is a switched linear state space model. A nonlinear model is obtained by allowing $\psi(j)$ and $L(j)$ to vary as a function of their respective error signals:

$$\psi(j) = \frac{\psi_\circ}{1 + b_w|e(j)|} \tag{3a}$$
$$L(j) = \frac{L_\circ}{1 + b_f|u_{im}(j)|} \tag{3b}$$

These nonlinear functions have the role of attenuating learning in response to large errors. For studies of short-term adaptation, the linear DO model uses five free parameters K, F, A_f, $\psi_\circ$, and $L_\circ$, while the nonlinear DO model uses two additional free parameters b_w and b_f. For studies of long-term adaptation, an additional parameter L_f is needed. The role of each parameter and its nominal value are shown in Table 1. A procedure to select the parameters is given in Section 3.5.

3.1 Overview of DO Model

The DO model consists of three conceptual pieces: (i) a fast reacting error feedback that responds to observed visual errors within a single trial; (ii) a slower reacting *disturbance observer* that monitors the environment to estimate any persistent visuomotor perturbation; (iii) an even slower *feedforward system* that learns from the disturbance observer over successive trials. As is indicated, (2a)-(2k) model the computations on trials when the cursor is visible. These computations include two indices k and j. The index k is incremented on every trial of the experiment, while index j is incremented in (2a) on every trial when a cursor is visible. Accordingly, variables indexed by k such as

$x(k)$ and $x_f(k)$ are updated on every trial, while variables indexed by j such as $e(j)$ and $u_s(j)$ are only updated on trials when a cursor is visible. Eq(2l)-(2o) model the computations performed on trials when no cursor is displayed.

We now explain the meaning of each computation. Eq(2b) specifies the manipulation imposed on the cursor as a function of the hand angle $x(k)$, the hand angle-gain α, and the perturbation $d(k)$. Eq(2c) models the *visual error* observed by the participant on the k-th trial. The scale factor α in (2b) introduces a *hand angle-gain* relative to the target. We restrict α to the range $\alpha \in [0, 1]$ in this paper. Its behavior has been described in Fig 2, which illustrates the impact of the hand angle-gain on the cursor's direction. First, consider the case when $d(k) = 0$. We can rewrite (2b) as:

$$\alpha = \frac{y(j) - r(k)}{x(k) - r(k)}$$

Thus, α determines the ratio of the cursor angle to the hand angle, both relative to the target angle. To compensate for this reduced angular gain, participants must produce a larger hand deviation - an effect illustrated in the right panel of Fig 2, with smaller α depicted by darker red arrows.

Returning to (2b), we have chosen not to scale $d(k)$ by α so that we can independently manipulate the hand angle-gain and the perturbation size in our experiments. An additional motivation for introducing α comes from considering its limiting values of $\alpha = 0$ or $\alpha = 1$. Suppose $\alpha = 0$, and $r(k) \equiv r$ and $d(k) \equiv d$, both constants. Then the cursor angle is

$$y(j) = r + d$$

which corresponds to an error clamp condition in which the cursor angle is independent of the hand angle. When $\alpha = 1$, the cursor position is

$$y(j) = x(k) + d$$

which corresponds to a standard visuomotor rotation paradigm (with $d = \pm 15°$ in the first two experiments). By decreasing α from 1 to 0, it becomes possible to gradually introduce an error clamp condition - referred to as a *graded error clamp*. The error clamp is known to elicit a saturated adaptive response [32, 34]; thus, varying α allows us to observe the emergence of nonlinear effects incrementally, across a series of experiments with different α values.

Now we turn to equations (2d), (2f), and (2g). Variables labeled with u represent components of the final motor command $u(k)$ which determines the hand movement on the next trial. The component defined in (2d) reflects an error feedback response that captures how the participant adjusts their movement following a visual error. This term models *single-trial learning* [35–37], and the parameter K can be interpreted as the participant's *error sensitivity* [38]. Next, the internal model component in (2f) is the output of a *disturbance observer* [39], and the subscript "im" may be interpreted in terms of either an *internal model* or an *implicit mechanism* (both interpretations are appropriate). Notably, $u_s(j)$ and $u_{im}(j)$ are only updated on trials where the cursor is visible. The overall motor command used on the next trial is given by (2g). It has two modes, depending on whether the participant is instructed to move the hand to the target or move the cursor to the target on the next trial. Specifically, $u_{im}(j)$ is used on trials where the participant is instructed to move the cursor to the target, while $x_f(k)$ is used on trials when the participant is instructed to move the hand to the target.

The final motor command defined in (2g) includes the sum $r(k) + u_f(k)$. The term $r(k)$ represents the target angle, and it models a motor subsystem that allows the participant

to move the hand to the target position with near-perfect accuracy, even without training. Accordingly, we assume that, in the absence of visual feedback and perturbation, at the start of an experiment the participant can reach the target reliably – apart from potential bias or noise, which are not included in the DO model. The term $u_f(k)$ is the output of a slowly adapting feedforward system and serves as a corrective signal that modifies the initial target-directed movement $r(k)$. This feedforward component also allows us to model the effect of *explicit re-aiming* used in other studies [29, 38, 40, 41]. If the participant is instructed to aim in a particular direction $r_{aim}(k)$ (relative to the target direction), then we replace $u_f(k)$ by $(r_{aim}(k) + u_f(k))$ in (2g) to reflect the instructed or cognitively acquired adjustment.

State updates are governed by (2h)-(2j). The disturbance observer state $w_0(j)$ is updated in (2h), while the feedforward system states $u_f(k)$ and $x_f(k)$ are updated in (2j) and (2i). Equation (2k) specifies the hand angle on the next trial, which is determined by the motor command formed using information from the previous trial.

We now turn to (2l)-(2o) which describe the computations on trials where no cursor is displayed. Since there is no visual error feedback on such trials, the disturbance observer does not update its states; both $w_0(j)$ and $\hat{w}(j)$ are held constant. This behavior reflects the assumption that participants cannot unlearn a visuomotor perturbation during no cursor trials - unlearning is presumed to require baseline trials with veridical visual feedback. However, in re-analyzing data from two previously published experiments, we found that incorporating a small forgetting factor ($F_n = 0.95$) for w_0 for no cursor trials improved the DO model's fit to participant behavior. This model extension will be discussed in Section 5. While the disturbance observer nominally remains quiescent during no cursor trials, the feedforward system continues to update in (2m)-(2n). Specifically, $u_f(k)$ is held constant, whereas $x_f(k)$ decays at a rate determined by parameter A_{fn}.

3.2 Disturbance Observer

The core computation of the DO model is performed by a *disturbance observer*, defined by (2e)-(2f) and (2h). Its function is to estimate any persistent exogenous disturbances affecting the visuomotor system. In the context of the visuomotor reaching task, such a disturbance corresponds to the perturbation $d(j)$. The key idea of a disturbance observer becomes evident over a sequence of trials with the cursor visible. To illustrate, consider the case where $r(k) \equiv r$ and $d(j) \equiv d$ are both constants. Also suppose $\alpha = 1$. For simplicity, assume that the cursor is visible on every trial, such that $j = k$. Under these assumptions, (2c) indicates that the visual error observed by the participant is

$$e(k) = r - x(k) - d\,.$$

The disturbance observer ((2e),(2f),(2h)) is updated when a cursor is visible, so the next update of $\hat{w}$ occurs on the next trial:

$$\begin{aligned}
\hat{w}(k+1) &= w_0(k+1) + Ge(k+1) \\
&= F(w_0(k) + Ge(k)) + G(u(k) - r(k) - u_f(k)) + Ge(k+1) \\
&= F\hat{w}(k) + G\big(u(k) - r - u_f(k) + r - x(k+1) - d\big) \\
&= F\hat{w}(k) + G\big(-d - u_f(k)\big)\,. \qquad (4)
\end{aligned}$$

This calculation shows that the hand movement $x(k)$ and the motor command $u(k)$ are effectively canceled through updates performed by the disturbance observer. This cancellation isolates the only unexpected component in the visual error, namely the

perturbation d. Specifically, the formula (4) with $F \in (0,1)$ is a stable filter. Assuming for the moment $u_f(k) \equiv 0$, this filter admits a well-defined steady state. Since $G = 1 - F$, the steady state value of $\hat{w}(k)$ is

$$\hat{w}_{ss} = \frac{G}{1-F}(-d) = -d\,. \tag{5}$$

This computation do not depend on the specific mode of the motor command $u(k)$; whether the participant is instructed to move the hand or the cursor to the target, the disturbance observer will still converge on an accurate estimate of the perturbation. The rate of convergence is governed by the parameter F. When the perturbation $d(j)$ varies over time or includes random fluctuations, then this disturbance observer will struggle to form a reliable estimate of the perturbation - consistent with empirical findings that environmental consistency facilitates learning [42–45]. Finally, (4) shows that the amount of the perturbation that must be accounted for by the disturbance observer is adjusted by the feedforward system output u_f.

In summary, under typical conditions in which the target position and perturbation are constant, $\alpha = 1$, the disturbance observer parameters satisfy $G = 1 - F$, and the feedforward component $u_f(k) \equiv 0$, the disturbance estimate $\hat{w}(k)$ converges to the negative of the perturbation (the case when $u_f(k) \neq 0$ is addressed in Section 4.7). This convergence is achieved using an *efference copy* of the motor command $u(k)$ and a measurement of the visual error $e(j)$. The persistent disturbance acting on the visuomotor system is then canceled using $u_{im}(j) = \psi(j)\hat{w}(j)$, where $\psi(j)$ is a scale factor that modulates the amount of learning at asymptote. If $\psi(j) \equiv 1$, the net effect of $u_{im}(j)$ is to drive the visual error to zero over successive Learn trials.

3.3 Feedforward System

The DO model includes a *feedforward system* described by (2i)-(2j). This system is responsible for gradually adapting the feedforward motor command $u_f(k)$ by way of a process of *learning transfer*, *consolidation of motor memory*, or *transfer of memory trace* [46–51]. As shown in (2i), this process is driven by a secondary error signal u_{im}, the output of the disturbance observer. The justification for interpreting u_{im} as an error signal from the point of view of the feedforward system is as follows. As shown in the preceding analysis, u_{im} asymptotically converges to the negative value of constant perturbations acting on the visual error. If such a perturbation persists, the disturbance observer must continuously compensate to maintain a properly calibrated visuomotor system. The magnitude of u_{im} quantifies this ongoing compensation effort. A sustained non-zero u_{im} thus informs the feedforward system that it requires a recalibration. In this way, the feedforward system can be viewed as a mechanism for gradually offloading the compensatory burden from the disturbance observer - potentially reducing the biological cost associated with maintaining long-term sensorimotor alignment.

For the feedforward system to operate properly, the *learning transfer rate* L_f should be sufficiently small. This constraint gives rise to a two timescale control architecture. The two timescale system operates as follows. When an environmental perturbation occurs, it is counteracted by the first responder available: $u_s(j)$. If the perturbation persists, then a somewhat slower but still short-term process is activated in $\hat{w}(j)$ to estimate and eliminate constant perturbations. As the disturbance observer output $u_{im}(j)$ accumulates information about the perturbation, this drives the activation of the state $x_f(k)$. The transfer of information from $u_{im}(j)$ to $x_f(k)$ is subject to strong saturation (3b), effectively constraining the extent of learning at this stage. A sustained positive or negative $x_f(k)$ drives the adaptation of $u_f(k)$. The role of $u_f(k)$ is to incorporate the

history of a persistent perturbation into the feedforward motor output, modifying it to the form $r(k) + u_f(k)$. The latter expression represents an updated motor command that reflects prolonged exposure to the visuomotor perturbation. More formally, the adaptation mechanism described by (2j) is such that $u_f(k)$ will asymptotically estimate $-d$. In turn, this means that the disturbance observer update computed in (2e) ultimately transforms to $\hat{w}(j+1) = F\hat{w}(j)$. That is, $\hat{w}(k)$ will decay to zero on a long timescale. In sum, $u_f(k)$ represents the system's long-term memory of the perturbation — an expression of savings — allowing for rapid reinstatement of compensatory behavior without re-learning.

3.4 Error Sensitivity Functions

The DO model includes three parameters K, $\psi(j)$, and $L(j)$, each of which may be interpreted as error sensitivity functions. The first, K corresponds to single trial or trial-to-trial learning [35, 36]; reflecting the system's immediate sensitivity to the observed visual error $e(j)$. Empirical studies have shown that this sensitivity decreases nonlinearly for larger errors, deviating from a strictly linear regime [35–37]. In the present model, this nonlinearity has not been implemented, so the error sensitivity function is a linear function of the error. The second error sensitivity function $\psi(j)$ accounts for *incomplete learning*, a phenomenon consistently observed in visuomotor adaptation tasks [31, 52–54]. The third function $L(j)$ represents the sensitivity to the secondary error $u_{im}(j)$, and it plays a key role in shaping the system's response under error clamp conditions [32, 34]. By modulating the gain on this pathway, $L(j)$ enables the DO model to replicate the plateauing of adaptation observed when the visual error is held constant.

	Parameter	Nominal Values	Role in Model
Disturbance observer	K	0.25	error sensitivity in single-trial learning
	F	$0.7 - 0.9$	learning rate
	F_n	0.95	forgetting rate during no cursor trials
	$\psi_\circ$	$0.9 - 1.0$	proportion of learning at asymptote
	b_w	0.001	saturation strength
Feedforward system	A_f	$0 - 0.9$	learning rate
	A_{fn}	0.95	forgetting rate during no cursor trials
	$L_\circ$	1.1	error sensitivity to u_{im}
	b_f	0.01	saturation strength
Long-term adaptation	L_f	0.0001	learning transfer rate

Table 1. Nominal model parameters

3.5 Selection of Parameters

We recommend an ordered procedure to select the parameters of the DO model consisting of three steps. Table 1 summarizes the parameters, their nominal values, and their functional roles. Additional guidance and empirical justification are provided in the Results section.

1. **Parameters for the disturbance observer.** The first step is to select parameters that govern the classical behaviors of visuomotor adaptation: savings

with counter perturbation, spontaneous recovery, and anterograde interference. These behaviors are particularly well-documented for the saccadic system [55] and in force field experiments [56, 57]. In the DO model these behaviors are captured by a linear disturbance observer with three free parameters: K, F, and $\psi_\circ$.

- Parameter K sets the gain for single trial learning. Across the experiments we considered, $K = 0.25$ is a reasonable nominal value, including for the saccadic system and visuomotor adaptation. This parameter is responsible for the inflection that was observed for the saccadic system and identified with arrows in Figure 3A of [55]. By making K larger, this inflection is made more pronounced, amplifying sensitivity to early errors.
- Parameter F sets the learning rate of the disturbance observer and must lie in the interval $(0, 1)$. It roughly corresponds to the learning rate of the slow process in a two-rate model (a coordinate transformation is needed to make the precise comparison). Our observation is that for visuomotor experiments with relatively fast learning, one can set $F = 0.7$. For the saccadic system as well as for force field experiments, the response is somewhat slower, so a value of $F = 0.9$ is more suitable. To accentuate the two rate classical behaviors of visuomotor adaptation, one should select a larger value of $F = 0.9$ to better separate the timescales in the two-rate model. Note that $G = 1 - F$, so it is not a free parameter.
- Parameter $\psi_\circ$ sets the fraction of learning at asymptote. When a participant fully compensates for the perturbation, then $\psi_\circ = 1$. However, many studies report incomplete learning [31, 52–54]. In this case a value of $\psi_\circ = 0.95$ is typical.

Once the parameters of a standard learning paradigm have been identified for a given experiment, these parameters should not be modified, as they fully characterize standard learning.

2. **Parameters for the feedforward system.** The feedforward system is active in trials with no cursor, zero error clamp trials, and trials with instructions to move the hand to the target (while ignoring the misaligned cursor). The linear feedforward system utilizes two parameters: A_f and $L_\circ$.

   - Parameter A_f determines the learning rate of the feedforward system. Based on analysis across multiple datasets, a nominal value is $A_f = 0.9$ provides a good approximation. However, there can be some variability in this parameter, which we report on below.
   - The parameter $L_\circ$ is the error sensitivity to the secondary error signal $u_{im}(\cdot)$. This parameter affects the steady state response of the feedforward system and is particularly relevant under error clamp conditions. It is best to calibrate $L_\circ$ using small error clamp values within the linear range of system response; see [34].

3. **Nonlinear model parameters.**

   For experiments involving non-zero error clamp trials in the nonlinear zone, it is necessary to introduce saturation in two areas of the DO model.

   - Parameter b_f controls the saturation behavior of the feedforward system under error clamp conditions. Specifically, it governs the nonlinear attenuation of steady state responses to sustained error signals. Increasing b_f amplifies the saturation effect, thereby reducing the asymptotic output of the

feedforward system. Because this parameter significantly shapes the DO model's behavior in the nonlinear regime, it should be used judiciously and only to capture empirical patterns specific to high-error clamp conditions. Notably, there is variability in reported steady state responses across studies: [34] documents higher asymptotic values than those observed in the similar experiment of [33]. As such, tuning b_f requires careful calibration against the particular experimental dataset being modeled.

- Parameter b_w constrains the growth of signals in the disturbance observer during non-zero error clamp trials. Without this constraint, the linear disturbance observer can produce unbounded growth of signals. Introducing nonlinear saturation via a small value of $b_w = 0.001$ effectively prevents divergence while leaving standard adaptation behavior unaffected. This ensures the DO model remains stable during prolonged clamp conditions without distorting its performance under typical learning paradigms.

3.6 Adaptation Fields

It is well known that the visuomotor system is able to perform dual adaptation, namely adaptation to two or more perturbations in the visual field [58–63]. The phenomenon is particularly evident when perturbations are associated with separate workspaces or targets [59–61]. The DO model presented here regards a single target and a single direction of the perturbation (CW or CCW). If one is interested to capture dual adaptation using the DO model, it is necessary to create separate computational modules for each adaptation field. Particularly, each adaptation field requires a dedicated disturbance observer to learn independent perturbations.

4 Results

We conducted a new experiment and also drew on datasets from both within and outside our lab to evaluate how well the DO model captures a range of phenomena in visuomotor adaptation. The first three sections - spontaneous recovery, savings, and the error clamp – address well-established behaviors and are therefore described briefly. Sections 4.4-4.7 focus on more complex behaviors that test the DO model's explanatory power, either through novel predictions or by accounting for effects not captured by other models. For consistency, all simulation plots show (primarily) positive hand angles to facilitate comparison.

4.1 Spontaneous Recovery

Spontaneous recovery is a rebound phenomenon that can be invoked in either washout, zero error clamp, or no cursor trials following a sufficiently long phase of Learn trials with a short counter-perturbation phase. Fig 5(a) depicts the classical mechanism of spontaneous recovery induced by a short counter-perturbation followed by a washout phase. This behavior is elicited in the DO model using only the disturbance observer. A separation of timescales between slow and fast processes is accentuated by slowing the disturbance observer learning rate to $F = 0.9$. Fig 5(b) illustrates evoked recovery [57], a more sophisticated form in which recovery emerges in no cursor trials, driven by the feedforward system. This highlights that spontaneous recovery can arise either from the disturbance observer or the feedforward system, depending on the context.

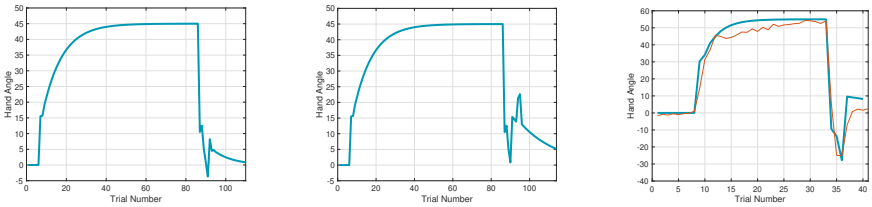

(a) Spontaneous recovery during washout. **(b)** Evoked recovery during no cursor trials. **(c)** Spontaneous recovery during zero error clamp.

Fig 5. Spontaneous Recovery. (a) Spontaneous recovery in an experiment of 80 Learn trials with a $-45°$ perturbation, 5 unlearning trials with a $+45°$ perturbation, and 20 washout trials with veridical feedback. (b) Evoked recovery in an experiment of 80 Learn trials with a $-45°$ perturbation, 4 unlearning trials with $+45°$ perturbation, 3 no cursor trials, 2 Learn trials with a $-45°$ perturbation, and 20 no cursor trials. (c) Spontaneous recovery in an experiment from [64] of 25 Learn trials with a $60°$ perturbation, 3 unlearning trials with a $-60°$ perturbation, and 5 zero error clamp trials. The red trace is the experimental data and blue traces are model predictions.

Fig 5(c) demonstrates another variant - spontaneous recovery elicited in zero error clamp trials - with simulation results compared to the data from [64]. To model zero error clamp trials, we follow the proposal of [65] that a brain process actively disengages at the transition from Learn trials to zero error clamp trials. Indeed, the error may be small at the end of a long sequence of Learn trials, yet when the zero error clamp is enforced, [65] shows that the hand angle decays. Additional evidence from [66] shows similar forgetting rates between no cursor trials and zero error clamp trials. Accordingly, we model zero error clamp trials as driven by the feedforward system, resulting in computations that are equivalent to no cursor trials.

4.2 Savings

Savings in the visuomotor system is a mechanism to perform recurring visuomotor tasks with improved performance and lower biological cost. It should be no surprise that savings is a multifaceted phenomenon, reflecting a multiplicity of strategies to achieve this desirable behavior, an idea supported by a range of sometimes conflicting experimental findings [67–70]. The DO model can reproduce at least four distinct forms of savings: (i) classical savings using counter-perturbations [56]; (ii) savings due to re-aiming [69]; (iii) savings due to increased error sensitivity [71]; and (iv) savings via learning transfer, which is addressed in Section 4.7. Figure 6 illustrates simulations of the first three mechanisms, with comparisons to experimental data from [68].

Fig 6(a) shows the classical notion of savings in a paradigm involving a brief counter-perturbation phase. The faster relearning in the second exposure to the perturbation arises because the disturbance observer retains information from the first learning phase. Due to its slower dynamics relative to the fast component $e(k)$, it partially retains this knowledge over the brief counter-perturbation. This savings mechanism is in accordance with the predictions of a two-rate model [56]. Fig 6(b) shows the effect of re-aiming on savings in Experiment 1 from [68]. Re-aiming is implemented in the second learning phase by setting $r_{aim}(k) = -\gamma d$ with $\gamma = 0.5$, where $\gamma \in (0, 1)$ specifies the proportion of the perturbation compensated through re-aiming. Fig 6(c) shows the effect of increased error sensitivity on savings. Increased error sensitivity is implemented in the DO model by increasing the model's error sensitivity parameter to $K = 0.5$ during the washout and second learning phases. The

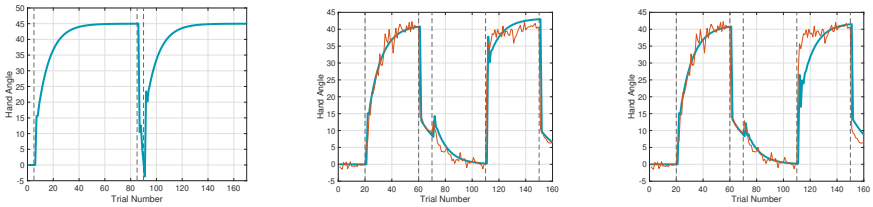

(a) Savings with counter-perturbation. **(b)** Savings with re-aiming. **(c)** Savings with increased error sensitivity.

Fig 6. Savings. (a) Savings in an experiment of 80 Learn trials with a $-45°$ perturbation, 5 unlearning trials with a $+45°$ perturbation, and 80 relearning trials. (b) Savings with re-aiming in Experiment 1 of [68] with 40 Learn cycles (4 targets per cycle) with a $-45°$ perturbation, 10 no cursor cycles, 40 washout cycles, and 10 no cursor cycles. (c) Savings with increased error sensitivity in Experiment 1 of [68]. Red traces correspond to experimental data and blue traces correspond to model predictions.

notion that the visuomotor system can adjust K is plausible and consistent with a *gain control mechanism* extensively investigated for the saccadic and smooth pursuit eye movement systems [72, 73].

4.3 Error Clamp

The error clamp paradigm offers a platform to explore nonlinear saturation in visuomotor adaptation. It has been observed over a number of studies that the amount of saturation at asymptote can be inconsistent [32–34]. The authors of [33] speculate this variability may stem from differences in experimental design - such as the use of endpoint versus continuous cursor feedback, or due to blanking the target after 250ms. While the DO model does not directly account for such experimental conditions, two parameters associated with the nonlinear feedforward system $L_\circ$, and b_f can be tuned to reproduce the range of behaviors observed under the error clamp. We use the data from [33] to illustrate the idea. Fig 7(a) compares the hand angle across three conditions: standard movement contingent learning, learning with instructions to move the hand to the target, and the error clamp with instructions to move the hand to the target; compare to Fig 1C of [32]. Fig 7(b)-(c) show simulations in the linear and saturated regimes of the error clamp; matching the behavioral profiles shown in Figs 1c-d of [34]. Fig 7(d) replicates the more suppressed response observed in [33]; this requires increasing the value of b_f, suggesting that this parameter is key to matching response magnitudes across different error clamp studies.

The DO model also accounts for error clamp behavior in cerebellar patients. In Experiment 3 of [32], a group of 10 participants with varying degrees of cerebellar ataxia performed an experiment with a $45°$ error clamp and instructions to move the hand to the target. Their responses (see Fig 3A of [32]) were clearly attenuated compared to controls. This outcome can be explained using the DO model by the fact that the feedforward system, which drives the computations when moving the hand to the target, requires as input u_{im} from the disturbance observer. We hypothesize the disturbance observer resides in the cerebellum (see the last section of the paper), so this output signal will either be absent or reduced in cerebellar patients, leading to diminished feedforward responses in the error clamp condition.

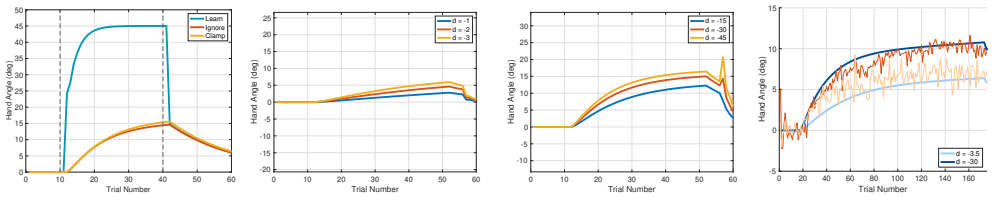

(a) **(b)** **(c)** **(d)**

Fig 7. Error Clamp. (a) Experiment 1 in [32] comparing Learn trials with a $-45°$ perturbation and instructions to move the cursor to the target; Ignore trials with instructions to move the hand to the target; and error clamp trials with a clamp size of $d = -45°$ with instructions to move the hand to the target. (b)-(c) Error clamp in the proportional (b) and saturated zones (c); see Figs 1c-d of [34]. (d) Experiment 1 of [33] using a cursor.

4.4 Graded Error Clamp

A central challenge in modeling visuomotor adaptation is to understand if the saturation behavior of the error clamp is an isolated phenomenon, a *singularity*, or if it is a ubiquitous phenomenon in all visuomotor tasks. To investigate this question, we designed a new experimental paradigm called the **graded error clamp**. This technique incrementally introduces error clamp conditions by adjusting a single parameter α which scales the contribution of the hand angle to the displayed cursor position. While similar scaling approaches have appeared in prior studies under the term "magnification of errors" [30, 31] (compare Eq 2 in [31] with our (2c)), to our knowledge this method has not previously been used to *gradually implement* the error clamp.

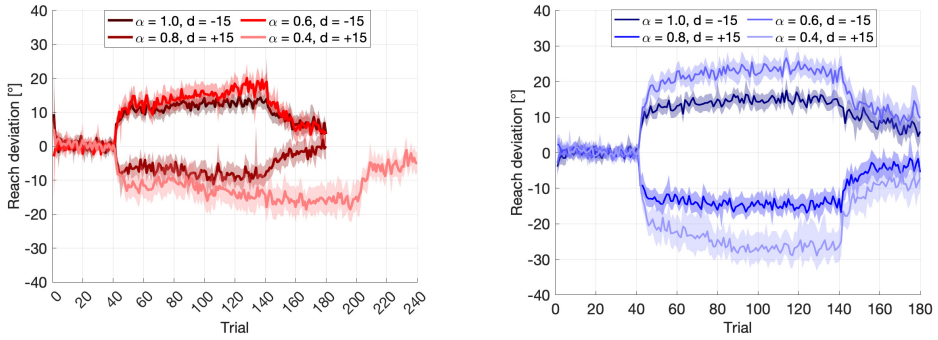

(a) Experiment 1: Move hand to target **(b)** Experiment 2: Move cursor to target

Fig 8. Graded Error Clamp. Mean angular reach deviations across participants in Experiments 1 and 2. (a) Experiment 1 consists of 40 baseline trials, 100 Ignore trials, and 40 no cursor trials. For $\alpha = 0.4$, the number of Ignore trials is 160. (b) Experiment 2 consists of 40 baseline trials, 100 Learn trials, and 40 no cursor trials. The perturbation is $-15°$ for $\alpha \in \{0.6, 1.0\}$ and $+15°$ for $\alpha \in \{0.4, 0.8\}$.

In our study, each participant performed the Ignore-N and Learn-N experiments in two sessions. As expected, we found no significant main effect of session or interaction between session and the other factors ($F(1, 29) = 0.07$, $p = 0.80$). Therefore, responses were averaged over the two sessions. During Ignore trials in the Ignore-N experiment, participants experienced a rotation of $-15°$ for $\alpha \in \{1.0, 0.6\}$ and $+15°$ for $\alpha \in \{0.8, 0.4\}$. The same rotation values were used in the Learn-N experiment during

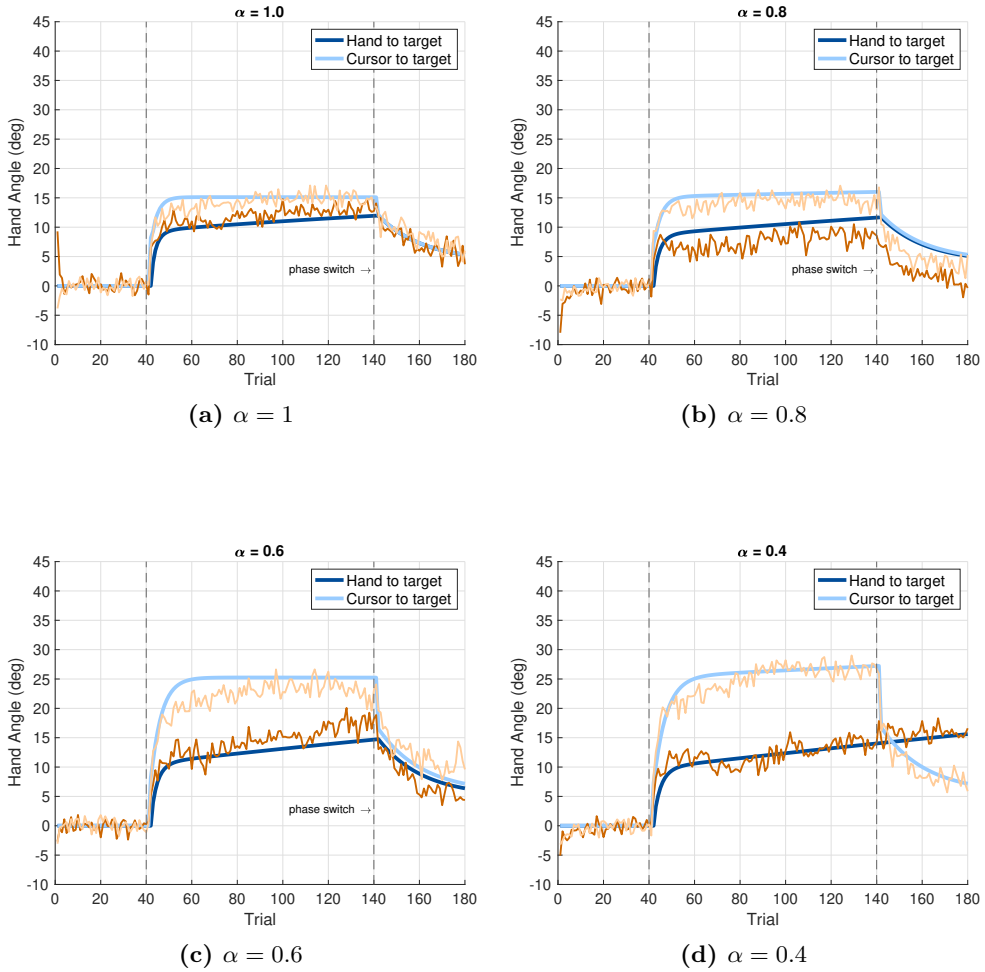

(a) $\alpha = 1$ **(b)** $\alpha = 0.8$

(c) $\alpha = 0.6$ **(d)** $\alpha = 0.4$

Fig 9. Graded Error Clamp. Simulation compared to experimental data in Experiments 1 and 2. A phase switch is predicted to occur at the transition from Learn to no cursor trials. Orange traces correspond to experimental data and blue traces correspond to model predictions.

Learn trials. The design is summarized in Fig 4. Fig 8 shows the mean reach deviation across all trial and experimental conditions.

Simulations corresponding to these two experiments are shown in Fig 9 superimposed with the experimental data. Data were separated by perturbation direction (CW and CCW) due to observed asymmetries in responses, particularly in the Learn-N experiment. In the Ignore-N experiment with instructions to move the hand to the target during Ignore trials, the DO model predicts that only the feedforward system makes a direct contribution to the hand movement. The response is suppressed relative to Learn-N experiment with the corresponding α value, as one would expect. According to the model, this suppressed response is due to the graded error clamp condition, which causes the nonlinear error sensitivity $L(j)$ to suppress the response of the feedforward system.

In the Learn-N experiment, the DO model predicts that the hand movement is driven by the disturbance observer. The feedforward system does not make a direct contribution during these trials, but becomes active during subsequent no cursor trials.

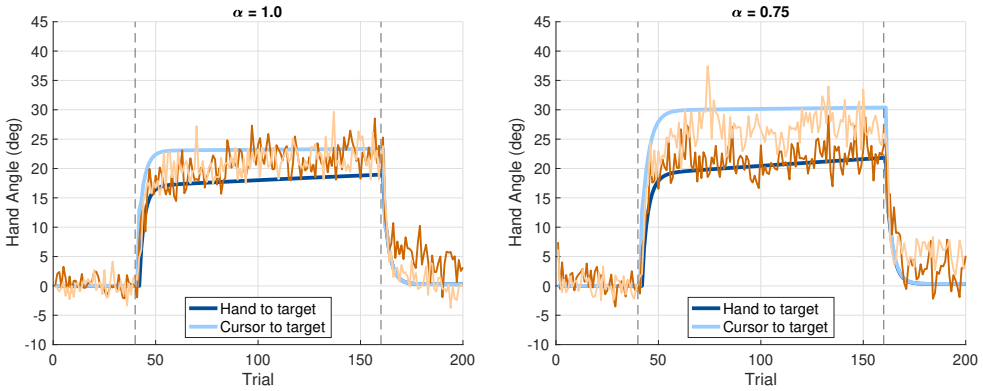

(a) $\alpha = 1$ **(b)** $\alpha = 0.75$

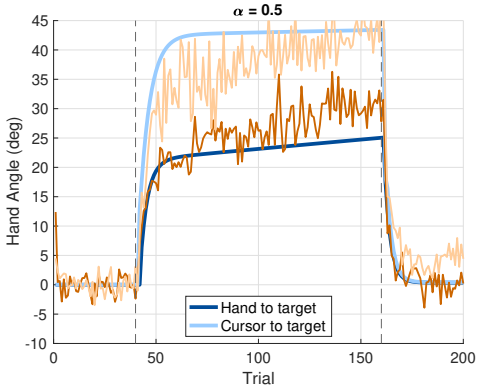

(c) $\alpha = 0.5$

Fig 10. Graded Error Clamp. Simulation compared to experimental data in Experiments 3 and 4. A phase switch is predicted to occur at the transition from Ignore to washout trials. Orange traces correspond to experimental data and blue traces correspond to model predictions.

To achieve zero steady state error in the Learn trials, the expected steady state value of the hand angle should be $x_{ss} = r - \frac{d}{\alpha}$. With the values $r = 90°$, $d = -15$, and $\alpha \in \{0.4, 0.6, 0.8, 1.0\}$, we expect $(x_{ss} - r) \in \{37.5, 25, 18.75, 15\}$. These steady state values of the hand angle are achieved in Experiment 2 for negative (CW) perturbations $d = -15$ corresponding to $\alpha \in \{1.0, 0.6\}$. However, for $\alpha \in \{0.4, 0.8\}$ and positive (CCW) perturbations of $d = +15$, we found participants did not fully compensate for the perturbation, and it was necessary to reduce the parameter $\psi_\circ$ in the DO model to a value $\psi_\circ = 0.8$ (from its nominal value of $\psi_\circ = 1$) in order to capture incomplete learning. This difference may reflect a well-known bias in visuomotor adaptation [74] where arm movements away from the saggital plane are suppressed due to the risk of generating inappropriate torques on the shoulder and elbow joints. The parameter $\psi_\circ$ may be viewed as a proxy for this safety mechanism. To better understand the results of the first two experiments, we conducted Experiments 3 (Ignore-W) and 4 (Learn-W), in which each participant only experienced one perturbation direction: either CW or CCW. This eliminated the possibility of carry-over between phases of the experiments. We found that the pattern of incomplete learning persisted for participants who

experienced CCW perturbations (a value of $\psi_\circ = 0.8$ again captures this incomplete learning in the DO model). Figure 10 shows the experimental results averaged over CW and CCW perturbations. We used a value of $\psi_\circ = 0.9$ in the DO model, corresponding to averaging responses with $\psi_\circ = 0.8$ (CCW) and $\psi_\circ = 1$ (CW).

4.5 Phase Switch Behavior

A **phase switch** is defined to be a switch in the *actively expressed* computational module or stream in the brain during visuomotor adaptation. The DO model includes two distinct computational modules that perform updates concurrently: a disturbance observer and a feedforward system. However, only one of these two processes is actively expressed in the motor command on any trial (as seen in (2g)). The DO model proposes that a phase switch occurs at the following experimental transitions:

- Learn trials to Ignore trials, and vice versa.
- Learn trials to no cursor trials without explicit instructions, where the absence of a cursor leads participants to default to moving their hand to the target.
- Learn trials to zero error clamp trials, as supported by findings in [65].

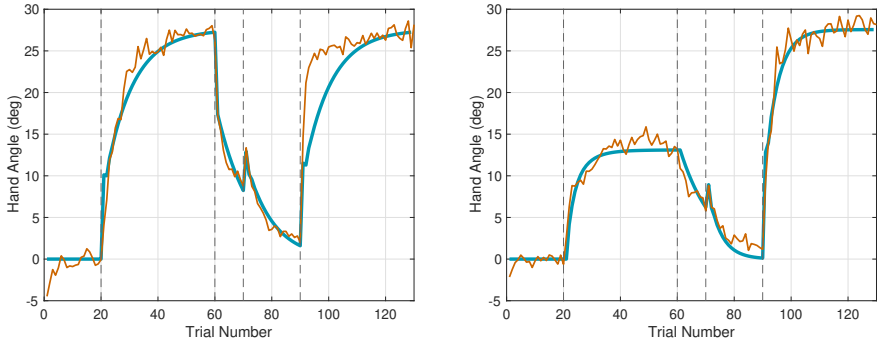

(a) Control group. **(b)** Clamp group.

Fig 11. Phase Switch. Demonstration of phase switches using Experiment 1 of [70]. Orange traces correspond to experimental data and blue traces correspond to model predictions.

The concept is illustrated using the data from [70]. Fig 11(a) shows their control group experiment consisting of 40 Learn trials, 10 no cursor trials, 20 washout trials, and 40 relearning trials. The DO model predicts two phase switches: one at the transition from Learn to no cursor trials, and the second from no cursor to washout trials. Fig 11(b) shows the clamp group experiment consisting of 40 error clamp trials, 10 no cursor trials, 20 washout trials, and 40 Learn trials. Here the DO model predicts only one phase switch at the transition from no cursor to washout phases.

Experiments 1-4 also demonstrate behavior attributable to a phase switch. In the Learn-N Experiment a phase switch is predicted to occur at the transition from Learn trials to no cursor trials, resulting in the characteristic drop in the hand angle, particularly visible for $\alpha = 0.4$. In the Ignore-N Experiment no phase switch is expected between Ignore and no cursor trials, leading to a smoother transition. In the Ignore-W Experiment, a phase switch is predicted between Ignore and washout trials, whereas the Learn-W Experiment is predicted to have no phase switch between Learn and washout

trials. In Experiments Ignore-W and Learn-W the discrepancy between a phase switch and no phase switch is more difficult to discern, likely because we used washout trials with veridical cursor feedback rather than no cursor trials, as in the Ignore-N and Learn-N Experiments.

One of the most compelling demonstrations of a phase switch is an experiment reported in [40]. In their Experiment 3, participants performed a sequence of Learn trials with a perturbation size $d \in \{15, 30, 45, 60, 90\}$, with one perturbation size for each group of participants. Following the Learn trials, participants performed a series of no cursor trials with instructions to move the hand directly to the target. It was shown in Fig 7A of [40] that aftereffect sizes in the no cursor phase did not significantly differ between groups who experienced different rotation sizes. The DO model accounts for this counterintuitive result by proposing the involvement of a hidden process during the Learn phase that becomes observable only after a phase switch at the onset of no cursor trials. Fig 12(a) presents simulations of this experiment, replicating the pattern reported in Fig 7A in [40]. The interpretation based on the DO model is that the hidden process is the feedforward system - it performs silent updates during Learn trials that are driven by the disturbance observer. These updates are not expressed behaviorally until the phase switch occurs, at which point the computations of the feedforward system are revealed.

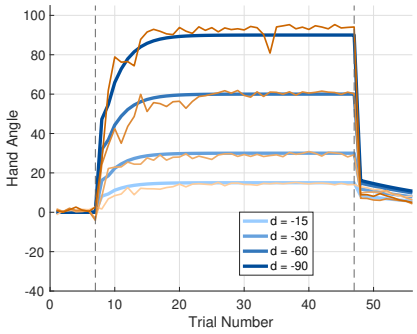

(a) Fig 7A of [40].

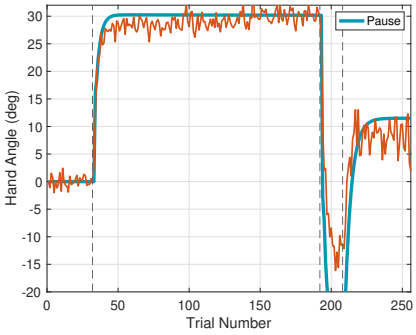

(b) Pause Experiment.

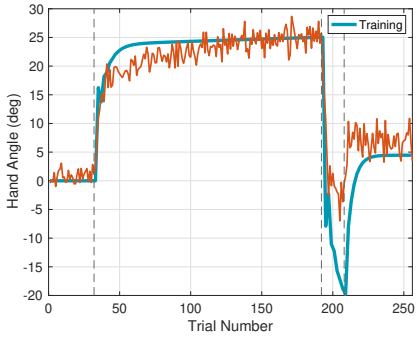

(c) Cursor trials.

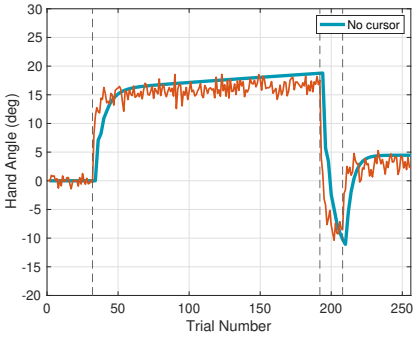

(d) No cursor trials.

Fig 12. Phase Switch. (a) Experiment 1 of [40]. (b) Pause Experiment of [28] with a brief pause after every Learn trial. (c) Cursor - No Cursor Experiment of [28], alternating Learn and no cursor trials. On odd-numbered Learn trials, participants were instructed to move the cursor to the target with the cursor visible. (d) On even-numbered no cursor trials, participants were instructed to move the hand to the target with no cursor. The perturbation size is 30°. Orange traces correspond to experimental data and blue traces correspond to model predictions.

Another striking demonstration of phase switch behavior comes from the experiment reported in [28] from our lab. This experiment belongs to a class of paradigms in which in which participants alternate between two types of trials: (1) moving a rotated cursor to the target with visual feedback, and (2) moving the unseen hand to the target with no visual feedback. The trial types alternate systematically — 30° rotated cursor trials followed by no cursor trials. This design is intended to measure implicit learning expressed during no cursor trials, arising from exposure to the rotated cursor during the preceding visual feedback trials.

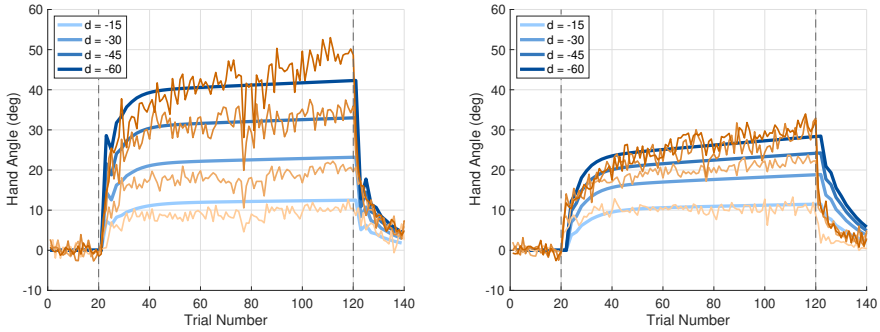

(a) Training trials **(b)** No cursor trials

Fig 13. Simulation of the experiment in [75] with rapid switching between cursor and no cursor trials. As in the study of [28], on (a) on odd-numbered training trials, participants are instructed to move the cursor to the target while the cursor is visible during and at the end of the reach; while (b) on even-numbered trials, participants are instructed to move the hand to the target while the cursor is not visible. In contrast with [28], the perturbation size is varied and also the length of the experiment is extended. The perturbation size for the training trials is shown on both figures. Orange traces correspond to experimental data and blue traces correspond to model predictions.

We hypothesize that this experiment induces a form of phase switching that continuously engages two distinct computational streams in the brain, each receiving input that conflicts with the subsequent trial's task demands. Given this conflict, it is not suprizing that some degree of interference arises - particularly when compared to standard 30° Learn phases that do not include interleaved no cursor trials (Fig 1A in [28]). Fig 12(b)-(d) show simulation results corresponding to the experiment in [28]. In Fig 12(b) participants perform a sequence of Learn trials, each followed by a brief pause. According to the DO model, only the disturbance observer is engaged, so there are no phase switches during the Learn and Unlearn phases of the experiment. We see that participants are able to compensate for the full 30° perturbation. Fig 12(c)-(d) provide evidence of interference between two processes. We see in Fig 12(c) that on cursor trials, the disturbance observer is not fully able to learn the 30° perturbation. Meanwhile, the feedforward system (whose output is depicted in Fig 12(d)) achieves a steady state around 15°, resembling behavior observed in error clamp conditions. This occurs because the feedforward system experiences an *effective error clamp* because the disturbance observer fails to vanquish the visual error. The effective clamped error in cursor trials is indistinguishable in the DO model from an experimentally imposed clamp condition, even though the former arises from a natural phenomenon of incomplete learning. The experiment further supports the view that the error clamp condition is a ubiquitous phenomenon that the feedforward system must continuously contend with under reasonably natural conditions.

We note that the DO model does not well-match the experimental data in the counter-perturbation phase of both the pause experiment and the cursor-no cursor experiments, as seen in Fig 12(b)-(c). Finally, Fig 13 shows simulation results for the experiment in [75] which has the same structure as the experiment in [28] but uses values of $d \in \{+15, +30, +45, +60\}$ (with $\alpha = 1$).

4.6 Explicit and Implicit Computations

The DO model may be utilized to analyze explicit and implicit contributions to visuomotor adaptation, a subject of significant interest in visuomotor learning [76]. Since the literature includes several interpretations of the terms "implicit" and "explicit", here we focus on an interpretation that the explicit part of adaptation regards that part of the motor command over which the participant has volitional control. The DO model suggests that the division between implicit and explicit components is somewhat more subtle than what is currently conceived. If we split the computations into two processes (the disturbance observer and the feedforward system), then the process whose computations are silent over a sequence of trials may appear to be implicit, even if those computations are revealed at a later phase in the experiment and can be altered by the participant.

In order to untangle this situation, we separately analyze Learn trials versus Ignore trials. We assume the number of trials is sufficiently small so that we can take $u_f(k) \equiv 0$. First, consider Learn trials when the participant is instructed to move the cursor to the target. A division of the motor command between explicit and implicit computations is

$$u(k) = u_{exp}(k) + u_{imp}(j) = \big(r(k) + u_s(j)\big) + u_{im}(j)\,.$$

The feedforward command $r(k)$ is explicit because the participant has efficacy to choose to reach to a specific target. The error feedback $u_s(j) = Ke(j)$ is also explicit based on an interpretation that the participant deliberately aims in the opposite direction of the perturbation by an amount that is a fraction of the observed error in the last reach. The computations of the disturbance observer are regarded as implicit, such that the participant has no authority to modify these computations - they progress automatically in a "machine-like" way.

This division follows the traditional view of implicit and explicit computations using a two-rate model. The implications will therefore be familiar. First, the explicit component makes a larger contribution at the beginning of learning when errors are large. The implicit component makes a relatively larger contribution near the end of learning when errors are small. Second, the explicit component makes a larger contribution when the perturbation is larger. Third, the explicit component has no aftereffects associated with it. Any aftereffects would be entirely attributable to $u_{im}(j)$ (we are speaking only about aftereffects following Learn trials, with the cursor always visible). Finally, if increased reaction time is associated with the explicit component, and increased aftereffect is associated with the implicit component, then certain experiments will result in a correlation between increased reaction time and decreased aftereffect.

Next, consider Ignore trials when the participant is instructed to move the unseen hand to the target. We propose that the motor command be split into explicit and implicit components as follows:

$$u(k) = u_{exp}(k) + u_{imp}(j) = \big(r(k) + r_{aim}(k)\big) + u_f(k)\,.$$

The component $r(k) + r_{aim}(k)$ is explicit because the participant still has the efficacy to choose to reach for a specific target as well as to use an aiming strategy. The

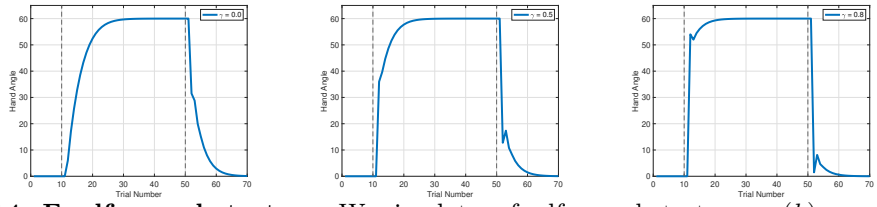

Fig 14. Feedforward strategy. We simulate a feedforward strategy $u_f(k) = r - \gamma \cdot d$ with $\gamma \in \{0, 0.5, 0.8\}$ to emulate an aiming strategy in which participants are informed of and compensate for a fraction of the perturbation during Learn trials. As γ is increased so that the motor command includes a larger explicit component, the learning rate increases, while aftereffects decrease.

component $u_f(k)$ generated by the feedforward system is implicit in the sense that this component cannot be suppressed by the participant, even if it results in movements that do not seem useful for the task (moving the hand to the target). Notice that when probing trials are used in visuomotor reach experiments, based on the available data, we believe participants are reporting the full motor command $r(k) + r_{aim}(k) + u_f(k)$. Participants may be aware of the implicit component $u_f(k)$ in their reporting, but they do not have the volition to alter or remove it.

Using these ideas, we may consider an experiment in which participants are instructed to deploy an aiming strategy based on information about the perturbation during Learn trials [77]. The DO model predicts that the motor command would be:

$$u(k) = r(k) + r_{aim}(k) + u_s(j) + u_{im}(j)\,,$$

with $r_{aim} = -\gamma \cdot d$ and $\gamma \in [0, 1]$ captures what fraction of the perturbation d the participant is informed about. Simulation results are shown in Figure 14 for three values of γ, and with $K = 0.1$ to accentuate the contribution of the aiming strategy. As γ is increased so that the motor command includes a larger explicit component, the learning rate increases, while the aftereffects decrease. We may compare these model predictions with the study in [77] that explored the relationship between reaction time, rate of decrease of errors, and aftereffects in a visuomotor reaching experiment with a perturbation of 60°. They found that a rapid decrease of errors was correlated with prolonged reaction times as well as reduced aftereffects. The participants with the longest reaction times exhibited the smallest aftereffects.

Longer reaction times are correlated with more emphasis on explicit strategies modeled by $u_{exp}(k)$. The DO model predicts that this component will reduce errors faster than a disturbance observer that operates on a (relatively) fixed learning rate determined by parameter F. Aftereffects arise in washout trials, and they correspond to unlearning in the disturbance observer of the previous 60° rotation. If the participant utilizes an explicit strategy, then the amount of learning to be performed by the disturbance observer is reduced, and this results in reduced aftereffects. The DO model does not capture any notion of time but we deduce from the discussions in [77] that explicit cognitive strategies take more time to constitute than the implicit component. See also the studies in [78] where further results (consistent with the study in [77]) on the role of explicit strategies are reported. A related and intriguing study is the one in [79] on decomposing explicit and implicit components of learning (with differing expressions of savings) as a function of preparation time.

4.7 Learning Transfer

Long-term adaptation has been described as a process that recalibrates motor skills, allowing the visuomotor system to adjust to changes in the body or environment without relearning from scratch [80]. In the study of [80] participants performed a visuomotor rotation task for one hour each day over five consecutive days. While participants demonstrated savings day to day, probing trials (in which participants indicated their intended aiming direction) revealed that participant's aiming direction remained constrained. These findings complicate efforts to model long-term adaptation. The DO model offers a candidate mechanism for long-term adaptation - referred to in this context as learning transfer - that helps account for recent experimental results.

In extended visuomotor experiments, the DO model captures the emergence of long term adaptation through (2j). During Learn trials, this component of the motor command continues to grow, despite the fact that $x_f(k)$ is limited due to the saturation imposed by $L(j)$. The parameter $L_f \ll 1$, so that (2j) represents a slow, long-term adaptation process. The combination of the short-term adaptation processes associated with $\hat{w}(j)$ and $x_f(k)$, combined with the long-term adaptation process for $u_f(k)$ gives rise to a two timescale system. This should not be confused with a traditional two-rate model; rather it reflects a layered architecture in which long-term learning gradually consolidates alongside faster, saturating processes.

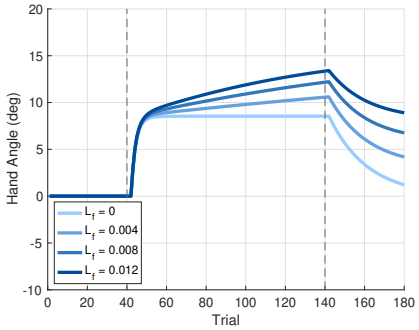

(a) Learning transfer in the Ignore-N Experiment with $\alpha = 1$.

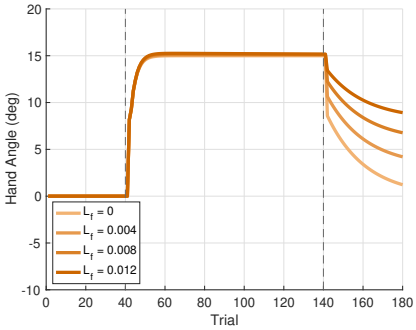

(b) Learning transfer in the Learn-N Experiment with $\alpha = 1$.

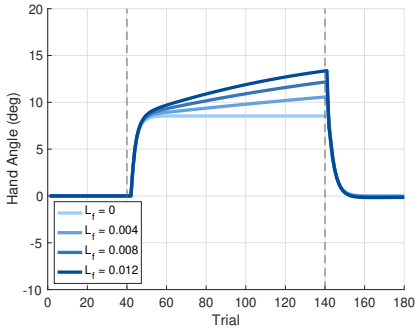

(c) Learning transfer in the Ignore-W Experiment with $\alpha = 1$.

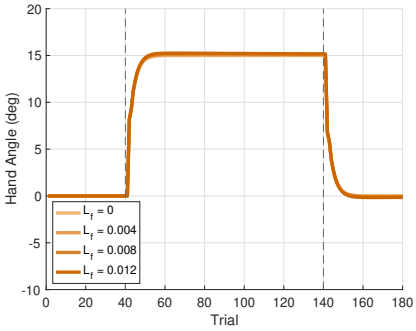

(d) Learning transfer in the Learn-W Experiment with $\alpha = 1$.

Fig 15. Learning transfer. Predicted behavior in Experiments 1-4 with $\alpha = 1$ as a function of the learning transfer rate L_f. All traces correspond to model predictions.

Figure 15 illustrates the DO model predictions for accelerated learning transfer in Experiments 1-4 with $\alpha = 1$ and increasing values of L_f, the rate of learning transfer. In Fig 15(a) (Ignore-N Experiment) two primary effects are observed in the simulations: (i) an increase in the slope of the response during Ignore trials, and (ii) an increase in the steady state response in the no cursor trials. In Fig 15(b) (Learn-N Experiment) there is no discernible effect during the Learn trials, as these are governed by the disturbance observer. However, the effect of increased learning transfer is revealed during the no cursor trials (following a phase switch) where the steady state response increases with increased values of L_f. Fig 15(c) (Ignore-W Experiment) shows that the slope of the response increases during the Ignore trials, but after a phase switch, no discernible effect is observed in the washout trials. In Fig 15(d) (Learn-W Experiment) there is no discernible effect because the Learn and washout trials are both governed by the disturbance observer, leaving the learning transfer process unexpressed.

We next examine experimental data for evidence supporting the DO model's predictions of learning transfer. Three datasets are potential candidates: the Ignore-N Experiment of the present study, the study reported in [28], and the study in [75]. Signs of learning transfer are present in all responses of Experiment 1, with the upward slope during Ignore trials particularly evident in Fig 9(c) with $\alpha = 0.6$. Additionally, the steady state hand angle during no cursor trials is non-zero, both for Experiments 1 and 2, consistent with the DO model. An exception is found in the Learn-N Experiment with $\alpha = 0.8$, where the hand angle returns to zero. Experiments 3-4 also exhibit evidence of learning transfer during Ignore trials, especially for $\alpha = 0.5$, as seen in Fig 10(c). Indeed, smaller α may induce stronger learning transfer. The study reported in [28], illustrated in Fig 12, reveals additional behaviors consistent with learning transfer, which we examine next.

The DO model predicts that learning transfer will produce a non-zero slope during both cursor and no cursor trials. It also predicts the emergence of a bias in the final phase of zero error clamp trials - a bias that unlike spontaneous recovery (which is transient) behavior) reflects a stable shift driven by learning transfer. According to the DO model, this bias will not develop in the absence of learning transfer. Finally, the study in [75] reveals yet another aspect of learning transfer. Here the DO model predicts that the slope of the response during no cursor (Ignore) trials increases with perturbation size - an effect observed in the experimental data in Fig 13. Taken together, these three experiments demonstrate that learning transfer can emerge within a single experimental session; it does not require days of experiments. It is possible that paradigms such as those used in [28] and [75] accelerate the transfer process through rapid phase switching between two computational processes that exchange information.

Although experimental evidence suggests that learning transfer can develop over a single session, the use of a two timescale architecture (with a small value of L_f) remains important for ensuring the stability of the system. Notably, the disturbance observer output $u_{im}(j)$ drives the update of the feedforward state $x_f(k)$ in (2i), which in turn drives the adaptation of $u_f(k)$ in (2j). However, $u_f(k)$ modulates the update of $\hat{w}(j)$, as computed in (4), thereby forming a closed feedback loop. If $u_f(k)$ were updated on the same timescale as $\hat{w}(j)$ and $x_f(k)$, then this closed-loop system could potentially introduce instability and generate runaway behavior. The slower adaptation rate governed by L_f thus serves as a stabilizing mechanism within the system.

4.8 Model of the Saccadic System

The DO model in (2) can be adapted to model the behavior of the saccadic system, specifically in *intersaccadic step* (ISS) experiments [55]. Below we outline how the DO model can be reformulated for this context. For the saccadic system the state $x(k)$ represents the saccade amplitude on the k-th saccade. The desired saccade amplitude on the k-th trial is given by $r(k) + d(k)$, where $r(k)$ denotes the nominal saccade size based on the location of a visual target relative to the initial eye position, and $d(k)$ represents a perturbation introduced by the experimenter while the k-th saccade is in progress. The visual error experienced by the participant at the end of the k-th saccade is therefore

$$e(k) = (r(k) + d(k)) - x(k)\,,$$

representing the mismatch between the required and actual saccade amplitude. To simplify the model for the saccadic system, we omit the feedforward system to focus on short-term adaptation. Also there is no need to differentiate visual feedback and no cursor trials in this context, so a separate index j is unnecessary.

A further consideration is that the saccadic system operates through *adaptation fields* - spatially localized, and often overlapping regions on the retina, each governed by its adaptation process. To isolate and model a single adaptation process, the range of saccade magnitudes $r(k)$ should be constrained to fall within a single adaptation field. For simplicity, we assume a constant saccade amplitude within this range such that $r(k) \equiv r$. The motor command for a given adaptation field includes a feedforward component that generates the appropriate movement for the nominal saccade size r. Thus, we set the feedforward term to be $u_f(k) = r$.

Collecting these adjustments, we arrive at a simplified model of the saccadic system for an adaptation field with a nominal saccade size r:

$$\begin{aligned}
e(k) &= r + d(k) - x(k) && \text{(6a)}\\
\hat{w}(k) &= w_0(k) + Ge(k) && \text{(6b)}\\
u_s(k) &= Ke(k) && \text{(6c)}\\
u_{im}(k) &= \psi(k)\hat{w}(k) && \text{(6d)}\\
u(k) &= r + u_s(k) + u_{im}(k) && \text{(6e)}\\
w_0(k+1) &= Fw_0(k) + FGe(k) + G(u_s(k) + u_{im}(k)) && \text{(6f)}\\
x(k+1) &= u(k) && \text{(6g)}
\end{aligned}$$

Here, $x(k)$ represents the executed saccade amplitude on trial k, $d(k)$ is the imposed perturbation during the saccade, and $e(k)$ is the visual error observed at the end of the movement. The term $u_{im}(k)$ captures short-term adaptive changes via a disturbance observer. The feedforward component $u_f(k) = r$ remains fixed for the adaptation field.

We can repeat the calculation of (4) for the disturbance observer in (6b) and (6f), assuming that $d(k) \equiv d$, a constant. We obtain

$$\begin{aligned}
\hat{w}(k+1) &= w_0(k+1) + Ge(k+1)\\
&= F\hat{w}(k) + G(u_s(k) + u_{im}(k)) + G(r + d - x(k+1))\\
&= F\hat{w}(k) + Gd
\end{aligned}$$

In this formulation, the disturbance observer learns to estimate $+d$. To model the saccadic system, we use the following nominal parameters values: $K = 0.22$, $F = 0.9$, $G = 1 - F$, and $\psi_\circ = 0.95$. Simulations of (6) successfully reproduce a range of hallmark behaviors observed in visuomotor adaptation: savings, reduced savings, anterograde interference, spontaneous recovery, rapid unlearning, and rapid downscaling [81].

5 Discussion

Researchers have long debated that multiple processes contribute to visuomotor adaptation [82]. This paper proposes a model composed of two interacting components. The primary mechanism is a disturbance observer that builds an internal model of persistent exogenous disturbance and reference signals acting on the visuomotor system based on visual error. A secondary mechanism - a feedforward system - learns from the output of the disturbance observer and is responsible for generating motor commands that position the hand at a specific spatial location. Functionally, the feedforward system plays a key role in offloading the steady state demands on the disturbance observer. We hypothesize that the disturbance observer is biologically expensive to operate over prolonged periods, and that the feedforward system serves to reduce this cost by gradually assuming control of learned behavior. This dynamic contributes to a division of labor between short-term, error-driven correction and longer-term consolidation.

The architecture of the DO model is characterized by a cascade structure: the disturbance observer drives the feedforward system, and sensory signals do not act directly on the feedforward system. This separation is crucial for reproducing several known behaviors in visuomotor learning. For example, it aligns with findings from [83] which showed that error sensitivity scales with perturbation consistency during Learn trials but not in Ignore trials - suggesting different computational pathways underlie these contexts, as captured in our model. Another key feature of the DO model is the concept of *phase switches* - transitions in the dominant computational process that occur in response to changes in task structure or sensory input. Here, we focused on phase switches triggered by instruction changes (e.g., from moving the cursor to the target to moving the hand directly) and by changes in visual feedback (e.g. removal or reintroduction of the cursor). These phase switches allow for context-dependent engagement of different modules within the visuomotor system. A more comprehensive classification of phase switch types - potentially involving implicit contextual cues, motor plan changes, or uncertainty - would be a valuable direction for future research.

One of the model's key predictions is that learning transfer is a meaningful and measurable phenomenon in visuomotor adaptation, with a distinctive behavioral signature. Specifically, it produces a gradual upward slope in hand angle during Ignore trials and a steady state bias in subsequent no cursor or zero error clamp trials. This dissociation underscores the importance of using trial structures that can selectively engage or reveal the contribution of the feedforward system - particularly when probing long-term or latent forms of adaptation.

5.1 DO Model Performance

Table 2 summarizes the parameter values used in the simulations. These values were not optimized in any formal sense; rather we selected nominal values that were sufficient to reproduce a wide range of qualitative behaviors across experiments. Notably, the parameters associated with the disturbance observer were remarkably stable across simulations. Slight variability was observed in the learning rate parameter F, which may reflect differences in experimental design - for example, the number of targets used, whether hand angles were averaged over targets, the use of continuous versus endpoint cursor feedback, or the duration of cursor visibility at the end of a reach. Parameter $\psi_\circ$ was used as a proxy for direction-dependent biases in learning. Specifically, we used $\psi_\circ = 0.8$ for CW perturbations, $\psi_\circ = 1.0$ for CCW perturbations, and $\psi_\circ = 0.9$ when averaging across both. These minor adjustments were sufficient to account for

incomplete adaptation effects and yielded consistent fits across studies. In contrast, greater variability was observed in the parameters associated with the feedforward system, particularly A_f and b_f. The variability in b_f mirrors the variability in the steady state behaviors reported for error clamp experiments [32–34], suggesting it may be tied to experimental protocols. Whether a canonical value of b_f exists remains an open question and may be resolved through additional experimental studies. The variability in A_f, however, points to a deeper issue: either the feedforward system is inherently more labile than the disturbance observer, or it reflects behavior that is not yet fully captured by the current DO model.

Table 2 also lists the experiments considered in this study, arranged roughly in order of increasing complexity from a modeling perspective. Classical behaviors such as savings, anterograde interference, and spontaneous recovery are governed by relatively few parameters and can often be reproduced using a standard two-rate model [56]. Evoked Recovery [57], the Bansal study [64], and the Bond and Taylor experiment [40] introduce additional complexity by probing aftereffects in no cursor or zero error clamp trials. These three experiments are predicted to involve a phase switch, whereby the parameters of the feedforward system play a central role in determining the magnitude of aftereffect or spontaneous recovery. The experiments listed near the bottom of Table 2 represent the highest level of complexity, as they require activation of all components of the DO model. In particular, the studies in [68] and [70] necessitated the introduction of a forgetting factor F_n in the disturbance observer state w_0 during no cursor trials. Specifically, the update rule $w_0(k+1) = F_n w_0(k))$ was applied to account for apparent decay in the perturbation estimate. However, we chose not to make this a permanent feature of the model, as these experiments likely involve multiple phase switches, the precise number and timing of which remain uncertain. We return to this issue next.

An important consideration when evaluating the DO model performance is the possibility that more phase switches occur than currently identified; see [66] for a related discussion. For example, in the study in [64] spontaneous recovery was observed in the zero error clamp trials following a learning phase and short unlearning phase. This spontaneous recovery can be explained in one of two distinct ways. One interpretation attributes spontaneous recovery to a form of memory retention within the feedforward system. Setting $A_f = 0.6$ to 0.9 allows the feedforward system to retain part of the learned response across the unlearning phase. The parameter b_f modulates the degree of saturation, shaping the amplitude of recovered responses. Thus, spontaneous recovery during the zero error clamp phase can be predicted by the interplay of two parameters: A_f, controlling retention, and b_f, controlling saturation.

An alternative explanation assumes no memory in the feedforward system so $A_f = 0$, and instead posits that spontaneous recovery arises from a phase switch between distinct internal models. Under this view, the short unlearning phase engages a second feedforward system that learns the reverse perturbation. When the zero error clamp trials are introduced, a phase switch returns the computations to the feedforward system of the first internal model. The change in error direction may serve as a trigger for this switch. Given the present state of knowledge, we assume that only a single internal model is active in this experiment. However, further studies are needed to determine whether multiple feedforward systems operate concurrently or sequentially in such paradigms, and to clarify the mechanisms that drive phase switching under these conditions.

One experiment among the group we examined where the DO model does not make correct predictions is the study of [28]. We see in Figs 12(b)-(c) that during cursor trials with a counter-perturbation, the DO model does not match the response. The pattern

of mismatch is the same pattern as in the Learn-N Experiment for CW v.s. CCW perturbations. To allow the model to match the experimental data, we may rescale the disturbance observer response using the parameter $\psi_\circ$ for the counter-perturbation phase. This phenomenon raises the question of whether the observed behavior reflects a phase switch to a different internal model that is not presently captured by the DO model. Thus, there would be two separate internal models to handle CW or CCW perturbations.

5.2 Comparison to Existing Models

5.2.1 Two-rate Model

Arguably the most influential model of sensorimotor adaptation is the two-rate model of [56]. This simple two state framework has proven remarkably effective in capturing a wide range of adaptive behaviors. Here we delve into the reason why this model is so resilient, using the saccadic system formulation in (6) as a starting point.

Let us assume that the perturbation is constant, $d(k) \equiv d$, and $\psi(k) \equiv \psi_\circ$. We identify the visual error $e(k)$ as the fast state, and the disturbance observer estimate $\hat{w}(k)$ as the slow state. Using this mapping, we can compute the updates for $\hat{w}(k+1)$ and $e(k+1)$ directly from (6), with the intent to recover the structure of the classical two-rate model within our more general framework. We obtain a two state linear model

$$e(k+1) = -Ke(k) - \psi_\circ \hat{w}(k) + d \tag{7a}$$
$$\hat{w}(k+1) = F\hat{w}(k) + Gd \tag{7b}$$

The first equation defines an error model that captures the evolution of the error. This equation explicitly includes the perturbation d, to reflect the fact that the perturbation acts externally on the system, shaping the error dynamics. These dynamics are clearly not internal to the brain; rather they unfold in the physical world but are observable as a measurement in the brain. The second equation captures the evolution of a brain state: the slow state $\hat{w}(k)$ which gradually estimates the perturbation by way of a simple filter operation. This internal estimation is achieved using both the observed error and an efference copy of the motor command.

While the system described in (7) captures core features of sensorimotor learning, it is not mathematically identical to the two-rate model in [56]. This highlights the point that the representation of learning processes depends on the choice of state variables, and that choice is not unique. The canonical two-rate model is typically written in the form

$$x_f(k+1) = A_f x_f(k) + B_f e(k) \tag{8a}$$
$$x_s(k+1) = A_s x_s(k) + B_s e(k)\,, \tag{8b}$$

where $x_f(k)$ and $x_s(k)$ denote fast and slow internal states, respectively, and the motor output $x(k)$ is the sum of these components. Both processes are driven by the same error signal and act in parallel to produce behavior.

In this formulation, the slow and fast states are typically treated as abstract brain states, without assigning them specific physiological or anatomical meaning. An important feature of (8b) is that the parameter A_s is always set to a value close to 1, reflecting slow retention dynamics. This choice is significant as it aligns with the internal model principle of control theory [25, 26]. In this context the principle asserts that that for the brain to learn and compensate for a constant perturbation d using only

error feedback, it must contain an internal model capable of generating constant signals. In control-theoretic terms, such a structure is known as an exosystem, and its canonical form is given by

$$w(k+1) = Sw(k)\,. \tag{9}$$

For this exosystem to generate constant signals, it is required that $S = 1$. In the two-rate model, this means A_s must be close to 1 in order to achieve an internal model of this exosystem. Equation (8b) is precisely the classical internal model introduced by E.J. Davison [84, Eq. 10], here for discrete-time systems. From a control theory perspective, the enduring success of the two-rate model lies in its ability to capture the fundamental - and mathematically necessary - requirement for an error-driven process to achieve perfect regulation in response to constant disturbances.

Returning to the DO model (2), the component that corresponds to the slow state of the two-rate model is the disturbance observer. This disturbance observer is itself a specific instantiation of an internal model, consistent with formulations from the control literature [39]. As such, there is a direct connection between three concepts: the slow state of the two-rate model, Davison's classical internal model, and the disturbance observer presented here. Furthermore, the disturbance observer used in the DO model is closely related to more advanced internal model designs used in adaptive control. These frameworks have been proposed to explain behavior in cerebellar regions such as the floccular complex [85, 86]. This connection opens the door for future comparisons between the DO model and biologically grounded models of cerebellar function. In summary, we see that the DO model can be viewed as an extension of the two-rate model, but with additional functionality. It incorporates a feedforward system to capture long-term learning and savings, introduces the capacity to model phase switches, and allows for nonlinear dynamics - capabilities that extend beyond the classical two-rate formulation.

5.2.2 Memory of Errors Model

The memory of errors (MoE) model, introduced in [87], is based on the principle that the brain can dynamically adjust the sensitivity to perceived errors. In this framework, persistent errors are assigned greater weight than variable or inconsistent errors, allowing the MoE model to explain phenomena such as saturation on single-trial learning [35]. The DO model does not include trial to trial modulation of error sensitivity. Instead, we assume a fixed sensitivity parameter K in the error feedback $u_s(j) = Ke(j)$. To remain within the linear range of this error sensitivity function, we deliberately chose small perturbation sizes in Experiments 1-4. Nonetheless, the structure of (2d) can be naturally extended to include saturation effects by allowing the error sensitivity parameter K to vary as a function of recent error history or magnitude. Such an extension could allow the DO model to account for trial-level nonlinearities and adapt more closely to the MoE framework, while preserving the architectural separation between disturbance estimation and feedforward adaptation.

The DO model (2) also incorporates two error sensitivity functions defined in (3a)-(3b), which bear conceptual similarity to the error sensitivity mechanisms proposed in the MoE model. A key distinction, however, is that the MoE model attributes error sensitivity to a population coding. In contrast, the DO model employs static error sensitivity functions that depend on the instantaneous error; they do not incorporate any temporal integration or memory of past errors. At this stage it remains unclear whether one approach offers a fundamentally more accurate description of neural error processing. While both frameworks can replicate key features of motor adaptation

behavior, their underlying mechanisms differ significantly. It is likely that future neurophysiological investigations - particularly those examining how error sensitivity is represented and modulated across different brain regions - will be required to adjudicate between these two accounts or to motivate a hybrid framework.

Finally, the MoE model also includes an explicit model of the environment, taking the form

$$\hat{w}(k+1) = A_s \hat{w}(k) + B_s e(k)\,.$$

As in previous models, the inclusion of an internal model within the MoE framework is necessary to satisfy the internal model principle. Specifically, accurate compensation for constant perturbations depends on incorporating an internal representation of the perturbation dynamics. This requirement is formalized by setting the adaptation parameter A_s close to or equal to 1. Only under this condition can the system achieve correct asymptotic behavior in response to constant disturbances.

5.2.3 COIN Model

The COIN model, introduced in [57], offers a distinct framework for understanding sensorimotor adaptation. In this model, each context has associated with it a scalar linear state equation that models a latent environmental quantity - such as the imposed perturbation in a visuomotor task. This formulation allows the model to maintain and update an arbitrarily large number of context-specific internal models. For each context, a corresponding observation provides a noisy replica of the context state, while a Kalman filter is employed to produce a noise-free estimate of the context state. The motor command is then computed as a weighted sum of these state estimates, where the weights correspond to the inferred probabilities (or responsibilities) of each context. Importantly, the model updates all contexts at each time step, scaling the updates by their respective inferred responsibilities.

There are several points of comparison between the DO model (2) and the COIN model. A point of commonality is that both models posit that multiple neural processes are updated in parallel and both allow for *silent* updates - i.e. changes in internal states that may not be immediately reflected in behavior. However, the models diverge in important ways. The COIN model is grounded in probabilistic reasoning for maintaining contexts, each associated with its own Kalman filter estimate and context probability. In contrast, the DO model operates deterministically and assumes a binary instructional context - whether the participant is instructed to move the hand or the cursor to the target - eliminating the need for probabilistic context inference.

A more profound difference between the DO model (2) and the COIN model regards the measurement structure. The COIN model assumes that the brain receives a noisy observation of each latent context state, enabling Kalman filters to denoise the signal. The DO model, on the other hand, relies solely on experimentally verifiable signals: the visual error and an efference copy of the motor command.

Another conceptual innovation in the DO model is the notion of a phase switch, which is a switch in the computational process governing motor output. This is distinct from a context switch, which refers to a change of external task conditions or instructions. For example, while a transition from Learn to washout trials represents a context switch, the underlying computations may remain unchanged - no phase switch occurs. Instead the transition from Learn to no visual feedback is both a context switch and a phase switch according to the model. Identifying and classifying the computational phase switches that occur during visuomotor adaptation is an important direction for future research.

5.2.4 CPC Model

A recently proposed framework is the cerebellar population coding (CPC) model [88] offering another biologically grounded approach to modeling sensorimotor adaptation. The CPC model is inspired by the Marr-Albus model of the cerebellum, but it also includes a model of plasticity in the deep cerebellar nuclei (DCN). The cerebellar cortex is hypothesized to act as an internal model to predict the sensory consequences of motor commands, positioning the cerebellum as either a forward or inverse model. The model adheres to cerebellar architecture in which Purkinje cell outputs project to the DCN.

A key architectural similarity between the DO model and the CPC model lies in their hierarchical (or cascade) structure. In the DO model, the feedforward system is driven by the disturbance observer, which is hypothesized to be implemented in the cerebellum. This mirrors the known anatomical pathway in which Purkinje cells project to the deep cerebellar nuclei (DCN), aligning with the CPC model's mapping of the cerebellar cortex and DCN roles. However, the DO model is a behavioral-level framework and does not place a restriction that the feedforward system resides entirely within the DCN. It may instead involve additional downstream structures, such as cortical motor areas. In this sense, the DO model maintains a more abstract relationship to cerebellar anatomy than the CPC model, which aims to more closely reflect the underlying neural circuitry. This distinction echoes the contrast between phenomenological and biophysical models of synaptic plasticity — where the former aim to capture functional behavior and the latter emphasize mechanistic fidelity.

A key distinction between the DO model and the CPC model lies in the interpretation of the visuomotor system's core computational function - particularly in regard to the cerebellum. We propose that the primary function of the cerebellum is to build internal models of persistent exogenous reference and disturbance signals in the environment, in line with the internal model principle of control theory [25, 26]. In contrast, the CPC model assumes the cerebellum builds forward (or inverse) models (putatively of the plant), thus estimating the current state of the effector (e.g. hand angle) given the motor command. In terms of expressive capability, the CPC model focuses exclusively on behaviors observed during error clamp conditions. The DO model is designed to capture a broader range of behaviors in visuomotor adaptation, including classical savings and spontaneous recovery, as well as more complex behaviors involving phase switches and long-term learning transfer. In particular, the CPC model does not a priori account for the results of Experiments 1-4, which go beyond a strict error clamp paradigm.

5.2.5 Summary of Comparison

To summarize our comparison with other models, we emphasize these metrics: (i) adherence to the internal model principle of control theory; (ii) biologically plausibility of the measurement structure; (iii) suitability of the control architecture; (iv) ability to capture learning transfer and phase switches; and (v) low-dimensional models.

We have discussed that the two-rate model can be interpreted as a sub-computation of the DO model. The DO model classifies the slow state $\hat{w}(k)$ as a brain state and the fast state $e(k)$ as measurable by the brain but evolving in the world, while the two-rate model blurs this boundary by considering only abstract states. The resilience of the two-rate model arises from its adherence (with a suitable parameter assignment) to the internal model principle; however, it was not conceived to capture learning transfer or phase switches. The MoM model, as a higher-order extension of the two-rate model, adheres to the internal model principle (via a so-called memory of the state of the

environment), well explains saturation in single-trial learning and certain types of savings, but does not capture learning transfer. We submit the latter behavior emerges strictly from a cascade architecture in which the error only enters the computations via the disturbance observer, not the feedforward system. The COIN model does not incorporate the internal model principle; consequently this model is forced to impose a biologically implausible assumption that a noisy measurement of the perturbation is already available in the brain. Instead, the DO model clarifies how a disturbance observer can reconstruct the perturbation using only sensory error and an efference copy of the motor command. Finally, the CPC model is based on a Marr-Albus framework to implement forward or inverse models (typically driven by prediction errors). Since the CPC model focuses only on error clamp behavior with instructions to ignore the cursor, it does not incorporate phase switches due to varying instructions or due to removal or reintroduction of the cursor. Similarly, learning transfer, a process involving learning the perturbation during either Learn or Ignore trials, is not captured in the CPC model. What is needed is a computation based on the internal model principle, such as a disturbance observer, that is invariant to the modality of the motor command.

5.3 Biological Plausibility

We have presented a discrete-time model of visuomotor adaptation in reach tasks. Like all biological discrete-time models, the formulation is necessarily abstract. Nevertheless, it is reasonable to ask whether the DO model components are biologically plausible.

The proposed disturbance observer is inspired by the adaptive internal model used to describe computations in the floccular complex [85, 86]. While an abstract discrete-time model, it may serve as a computational blueprint for cerebellar contributions to visuomotor adaptation [89]. For instance, the stable filter in (2h) may represent filtering in the cerebellar granular layer. The signal $u(k)$, which drives this filter, aggregates multiple classes of mossy fiber inputs, including the component $u_{im}(j)$ that reaches the cerebellar component via the nucleo-cortical pathway [90–93]. The visual error signal $e(j)$, critical for adaptation, could arise from activity in regions such as the superior colliculus as well as the frontal eye fields of the frontal cortex. Although the DO model does not explicitly represent the climbing fiber input as well as synaptic plasticity at parallel fiber - Purkinje cell synapses, these elements are essential in cerebellar learning. Prior work has modeled adaptation at these synapses as a slower process [81]. Further research is needed to bridge differences between the internal model used for the floccular complex and one that supports visuomotor adaptation. The nonlinear error sensitivity in (3a) may reflect modulatory input from the nucleoolivary pathway, which is known to to suppress cerebellar activity [47, 94, 95]. The parameter $\psi(j)$ may be interpreted as a form of error gating or safety control, limiting unstable behavior in the internal model. Biologically, this would require graded inhibition in the inferior olive [96–98].

At present, the anatomical substrate for the feedforward system remains less certain. Due to its simplicity in the DO model, we can only speculate at this point. One might assign this role to the dentate nucleus, analogous to the manner in which learning transfer occurs from the Purkinje cells of the floccular complex to the medial vestibular nucleus [46, 48, 51, 99]. Alternatively, downstream targets of the dentate nucleus—including primary motor cortex (M1), prefrontal cortex, and posterior parietal cortex—may also contribute to feedforward computations [100, 101].

6 Conclusion

In this project we set out to explain various phenomena in visuomotor adaptation using a disturbance observer based model, a relatively recent innovation in control theory. The resulting DO model has three main components: a fast reacting error feedback, a somewhat slower disturbance observer, and a feedforward system that learns from the disturbance observer. The motor command switches between the output of the disturbance observer and the feedforward system, depending on the instructions to the participant to move either the hand or the cursor to the target. This discrete time model is necessarily a simplification, but its development has been guided by biological principles and anatomical structure. Initial model parameters for the error feedback and disturbance observer were based on previous literature; the error feedback is derived from single-trial learning and the disturbance observer model has strong ties to the well-established two-rate model. A key feature of the DO model is its cascade architecture, in which the feedforward system does not directly sense the visual error, but rather it learns from the disturbance observer.

Using the DO model we can explain several forms of spontaneous recovery, several types of savings, error clamp behavior, behaviors arising from switching between instructions, and explicit and implicit computations. We also expose several new behaviors. We introduce a novel experimental paradigm called the graded error clamp to explore the emergence of error clamp behavior over a sequence of experiments, by varying a single parameter that scales the hand angle. We introduce the notion of a phase switch, and we identify several forms of phase switches, based on current datasets. We introduce learning transfer in visuomotor adaptation, and we fully characterize its signature behaviors. The DO model does not fully capture experiments involving both counterclockwise and clockwise rotations, indicating that an extension with separate disturbance observers for each direction may be required. Exploring this possibility is left for future work. The DO model compares well in terms of its expressive capabilities relative to existing models; nevertheless, we see it as a complementary tool for further study. It utilizes a control architecture that mimics the computations in the floccular complex and medial vestibular nucleus for the slow eye movement systems, a forward step toward unveiling the computations of the cerebellum.

Most importantly, our disturbance observer framework offers a new perspective from control theory that should be considered in modeling visuomotor adaptation.

Acknowledgments

We acknowledge the generous support of the Government of Canada's New Frontiers in Research Fund (NFRF), (NFRFE-2021-00458).

Author Contributions

Conceptualization: Mireille E. Broucke, Bernard M. t'Hart, Denise Y.P. Henriques, Jean-Jacques Orban de Xivry

Data collection and analysis: Gaurav Sharma

Funding acquisition: Mireille E. Broucke, Denise Y.P. Henriques

Writing - original draft: Mireille E. Broucke, Gaurav Sharma

Writing - review & editing: Mireille E. Broucke, Bernard M. t'Hart, Denise Y.P. Henriques, Jean-Jacques Orban de Xivry

References

1. Galea J, Vazquez A, Pasricha N, Orban de Xivry J, Celnik P. Dissociating the roles of the cerebellum and motor cortex during adaptive learning: the motor cortex retains what the cerebellum learns. Cerebral Cortex. 2011;21:1761–1770.
2. Haith AM, Krakauer JW. Model-based and model-free mechanisms of human motor learning. Adv Exp Med Biol. 2013;782:1–21.
3. Izawa J, Shadmehr R. Learning from Sensory and Reward Prediction Errors during Motor Adaptation. PLoS Computational Biology. 2011;7(3).
4. Uehara S, Mawase F, Celnik P. Learning Similar Actions by Reinforcement or Sensory-Prediction Errors Rely on Distinct Physiological Mechanisms. Cerebral Cortex. 2018;28:3478–3490.
5. Morehead JR, Orban de Xivry JJ. A Synthesis of the Many Errors and Learning Processes of Visuomotor Adaptation. bioRxiv. 2021;doi:10.1101/2021.03.14.435278.
6. Vandevoorde K, Orban de Xivry JJ. Internal model recalibration does not deteriorate with age while motor adaptation does. Neurobiology of Aging. 2019;80:138–153.
7. Spampinato D, Celnik P. Multiple motor learning processes in humans: their neurophysiological bases. The Neuroscientist. 2021;27(3):246–267.
8. Tzvi E, Loens S, Donchin O. Mini-review: the role of the cerebellum in visuomotor adaptation. The Cerebellum. 2022;21:306–313.
9. Scott S. Optimal feedback control and the neural basis of volitional motor control. Nature Reviews. 2004;5:534–546.
10. Huang H, Kram R, Ahmed A. Reduction of Metabolic Cost during Motor Learning of Arm Reaching Dynamics. Journal of Neuroscience. 2012;32(6):2182–2190.
11. Crevecoeur F, Sepulchre RJ, Thonnard JL, Lefèvre P. Improving the state estimation for optimal control of stochastic processes subject to multiplicative noise. Automatica. 2011;47(3):591–596.
12. Kawato M, Gomi H. A computational model of four regions of the cerebellum based on feedback-error learning. Biological Cybernetics. 1992;68:95–103.
13. Gomi H, Kawato M. Adaptive feedback control models of the vestibulocerebellum and spinocerebellum. Biological Cybernetics. 1992;68:105–114.
14. Jordan M, Rumelhart D. Forward models: supervised learning with a distal teacher. Cognitive Science. 1992;16:307–354.
15. Miall RC, Wolpert DM. Forward models for physiological motor control. Neural Networks. 1996;9(8):1265–1279.

16. Kawato M. Internal models for motor control and trajectory planning. Current Opinion in Neurobiology. 1999;9(6):718–727.

17. Orban de Xivry JJ, Ethier V. Neural correlates of internal models. Journal of Neuroscience. 2008;28:7931–7932.

18. Wolpert D, Ghahramani Z, Jordan M. An internal model for sensorimotor integration. Science. 1995;269(5232):1880–1882.

19. Wolpert D, Miall C, Kawato M. Internal models in the cerebellum. Trends in Cognitive Sciences. 1998;2(9):338–347.

20. McNamee D, Wolpert D. Internal Models in Biological Control. Annual Reviews in Control, Robotics, and Autonomous Systems. 2019;2:339–364.

21. Crevecoeur F, Thonnard JL, Lefèvre P. Forward models of inertial loads in weightlessness. J Neuroscience. 2009;161(2):589–598.

22. Widrow B, Stearns S. Adaptive Signal Processing. Prentice-Hall; 1985.

23. Dean P, Porrill J. Adaptive filter models of the cerebellum: computational analysis. Cerebellum. 2008;7:567–571.

24. Porrill J, Dean P, Anderson S. Adaptive filters and internal models: multilevel description of cerebellar function. Neural Networks. 2013; p. 134–149.

25. Francis B, Wonham WM. The internal model principle for linear multivariable regulators. Applied Mathematics and Optimization. 1975;2(2):170–194.

26. Francis B, Wonham WM. The internal model principle of control theory. Automatica. 1976;12:457–465.

27. Nashed J, Crevecoeur F, Scott S. Rapid Online Selection between Multiple Motor Plans. Journal of Neuroscience. 2014;34(5):1769–1780.

28. Ruttle J, 't Hart BM, Henriques D. Implicit motor learning within three trials. Scientific Reports. 2021;11(1627).

29. 't Hart BM, Taqvi U, Gastrock RQ, Ruttle JE, Modchalingam S, Henriques DYP. Measures of Implicit and Explicit Adaptation Do Not Linearly Add. eNeuro. 2024;11(8).

30. Patton J, Wei Y, Bajaj P, Scheidt R. Visuomotor Learning Enhanced by Augmenting Instantaneous Trajectory Error Feedback during Reaching. PLoS ONE. 2013;8(1):e46466.

31. van der Kooij K, Brenner E, van Beers R, Smeets J. Visuomotor adaptation: how forgetting keeps us conservative. PLoS One. 2015;10(2).

32. Morehead R, Taylor J, Parvin D, Ivry R. Characteristics of implicit sensorimotor adaptation revealed by task-irrelevant clamped feedback. Journal of Cognitive Neuroscience. 2017;29(6):1061–1074.

33. Tsay T, Avraham G, Kim H, Parvin D, Wang Z, Ivry R. The effect of visual uncertainty on implicit motor adaptation. Journal of Neurophysiology. 2021;125:12–22.

34. Kim H, Morehead R, Parvin D, Moazzezi R, Ivry R. Invariant errors limitations in motor correction rather than constraints on error sensitivity. Communications Biology. 2018;1(19).

35. Wei K, Kording K. Relevance of Error: What Drives Motor Adaptation? Journal of Neurophysiology. 2009;101(2):655–664.

36. Fine M, Thoroughman K. Motor adaptation to single force pulses: sensitive to direction but insensitive to within-movement pulse placement and magnitude. Journal of Neurophysiology. 2006;96:710–720.

37. Marko M, Haith A, Harran M, Shadmehr R. Sensitivity to prediction error in reach adaptation. Journal of Neurophysiology. 2012;108:1752–1763.

38. Hutter S, Taylor J. Relative sensitivity of explicit reaiming and implicit motor adaptation. Journal of Neurophysiology. 2018;120:2640–2648.

39. Nikiforov V, Gerasimov D. Adaptive Regulation. vol. 491. Switzerland: Springer International Publishing; 2022.

40. Bond K, Taylor J. Flexible explicit but rigid implicit learning in a visuomotor adaptation task. Journal of Neurophysiology. 2015;113:3836–3849.

41. McDougle S, Ivry R, Taylor J. Taking Aim at the Cognitive Side of Learning in Sensorimotor Adaptation Tasks. Trends in Cognitive Sciences. 2016;20(7):535–544.

42. Cassanello C, Ohl S, Rolfs M. Saccadic adaptation to a systematically varying disturbance. Journal of Neurophysiology. 2016;116:336–350.

43. Castro LG, Hadjiosif A, Hemphill M, Smith M. Environmental consistency determines the rate of motor adaptation. Current Biology. 2014; p. 1050–1061.

44. Karniel A, Mussa-Ivaldi F. Sequence, time, or state representation: how does the motor control system adapt to variable environments? Biological Cybernetics. 2003;89(1):10–21.

45. Havermann K, Lappe M. The Influence of the Consistency of Postsaccadic Visual Errors on Saccadic Adaptation. Journal of Neurophysiology. 2010;103(6):3302–3310.

46. Broussard D, Kassardjian C. Learning in a simple motor system. Learning and Memory. 2004;11(2):127–136.

47. Herzfeld D, Hall N, Tringides M, Lisberger S. Principles of operation of a cerebellar learning circuit. eLife. 2020;9:e55217.

48. Kassardjian C, Tan Y, Chung J, Heskin R, Peterson M, Broussard D. The site of a motor memory shifts with consolidation. Journal of Neuroscience. 2005;25(35):7979–7985.

49. Lisberger S, Pavelko T, Broussard D. Neural basis for motor learning in the vestibuloocular reflex of primates. I. Changes in the responses of brain stem neurons. Journal of Neurophysiology. 1994;72(2):928–953.

50. Nagao S, Honda T, Yamazaki T. Transfer of memory trace of cerebellum-dependent motor learning in human prism adaptation: A model study. Neural Networks. 2013;47:72–80.

51. Shutoh F, Ohki M, Kitazawa H, Itohara S, Nagao S. Memory trace of motor learning shifts transsynaptically from cerebellar cortex to nuclei for consolidation. Neuroscience. 2006;139:767–777.

52. Shmuelof L, Hang V, Haith A, Dekicki R, Mazzoni P, Krakauer J. Overcoming motor forgetting through reinforcement of learned actions. Journal of Neuroscience. 2012;32:14617–14621.

53. Vaswani P, Shmuelof L, Haith A, Deknicki R, Huang V, Mazzoni P, et al. Persistent residual errors in in motor adaptation tasks: reversion to baseline and exploratory escape. Journal of Neuroscience. 2015;35(17):6969–6977.

54. Langsdorf L, Maresch J, Hegele M, McDougle S, Schween R. Prolonged response time helps eliminate residual errors in visuomotor adaptation. Psychonomic Bulletin & Review. 2021;28:834–844.

55. Kojima Y, Iwamoto Y, Yoshida K. Memory of learning facilitates saccadic adaptation in the monkey. Journal of Neuroscience. 2004;24(34):7531–7539.

56. Smith M, Ghazizadeh A, Shadmehr R. Interacting adaptive processes with different timescales underlie short-term motor learning. PLOS Computational Biology. 2006;4(6).

57. Heald JB, Lengyel M, Wolpert D. Contextual inference underlies the learning of sensorimotor repertoires. Nature. 2021;600:489–493.

58. Ayala M, Henriques D. Differential contributions of implicit and explicit learning mechanisms to various contextual cues in dual adaptation. PLoS ONE. 2021;16(7):e0253948.

59. Baldeo R, Henriques D. Dual adaptation to opposing visuomotor rotations with similar hand movement trajectories. Exp Brain Res. 2013;227:231–241.

60. Woolley D, Tresilian J, Carson R, Riek S. Dual adaptation to two opposing visuomotor rotations when each is associated with different regions of workspace. Exp Brain Res. 2007;179:155–165.

61. Woolley D, Rugy A, Carson R, Riek S. Visual target separation determines the extent of generalisation between opposing visuomotor rotations. Exp Brain Res. 2011;212:213–224.

62. Hegele M, Heuer H. Implicit and explicit components of dual adaptation to visuomotor rotations. Consciousness and Cognition. 2010;19:906–917.

63. Pearson T, Krakauer J, Mazzoni P. Learning not to generalize: modular adaptation of visuomotor gain. J Neurophysiology. 2010;103:2938–2952.

64. Bansal A, 't Hart B, Cauchon U, Eggert T, Straube A, Henriques DYP. Motor adaptation does not differ when a perturbation is introduced abruptly or gradually. Exp Brain Res. 2023;241:2577–2590.

65. Vaswani R, Shadmehr R. Decay of motor memories in the absence of error. Journal of Neuroscience. 2013;33(18):7700–7709.

66. Kitago T, Ryan S, Mazzoni P, Krakauer J, Haith A. Unlearning versus savings in visuomotor adaptation: comparing effects of washout, passage of time, and removal of errors on motor memory. Frontiers in Human Neuroscience. 2013;7(307).

67. Krakauer J, Ghez C, Ghilardi M. Adaptation to visuomotor transformations: consolidation, interference, and forgetting. Journal of Neuroscience. 2005;25(2):473–478.

68. Avraham G, Morehead J, Kim H, Ivry R. Reexposure to a sensorimotor perturbation produces opposite effects on explicit and implicit learning processes. PLoS Biology. 2021;19(3).

69. Morehead R, Qasim S, Crossley M, Ivry R. Savings upon re-aiming in visuomotor adaptation. Journal of Neuroscience. 2015;35(42):14386–14396.

70. Yin C, Wei K. Savings in sensorimotor adaptation without an explicit strategy. Journal of Neurophysiology. 2020;123(3):1180–1192.

71. Herzfeld D, Vaswani P, Marko M, Shadmehr R. A memory of errors in sensorimotor learning. Science. 2014;345:1349–1353.

72. Brostek L, Eggert T, Glasauer S. Gain control in predictive smooth pursuit movements: evidence for an acceleration-based predictive mechanism. eNeuro. 2017;4(3):1–13.

73. Nuding U, Ono S, Mustari M, Buttner U, Glasauer S. A theory of the dual pathways for smooth pursuit based on dynamic gain control. Journal of Neurophysiology. 2008;99(6):2798–2808.

74. Ghilardi M, Gordon J, Ghez C. Learning a Visuomotor Transformation in a Local Area of Work Space Produces Directional Biases in Other Areas. Journal of Neurophysiology. 1995;73(6):2535–2539.

75. D'Amario S, Ruttle J, 't Hart BM, Henriques D. Implicit Adaptation is Fast, Robust and Independent from Explicit Adaptation. bioRxiv. 2024;.

76. de Brouwer A, Albaghdadi M, Flanagan J, Gallivan J. Using gaze behavior to parcellate the explicit and implicit contributions to visuomotor learning. Journal of Neurophysiology. 2018;120:1602–1615.

77. Fernandez-Ruiz J, Wong W, Armstrong I, Flanagan JR. Relation between reaction time and reach errors during visuomotor adaptation. Behavioural Brain Research. 2011;219:8–14.

78. Neville K, Cressman E. The influence of awareness on explicit and implicit contributions to visuomotor adaptation over time. Experimental Brain Research. 2018;236(7):2047–2059.

79. Haith AM, Huberdeau DM, Krakauer JW. The influence of movement preparation time on the expression of visuomotor learning and savings. J Neuroscience. 2015;35:5109–5117.

80. Wilterson S, Taylor J. Implicit visuomotor adaptation remains limited after s everal days of training. eNeuro. 2021;8(4).

81. Gawad A, Broucke ME. Visuomotor Adaptation is a Disturbance Rejection Problem. In: IEEE Conference on Decision and Control; 2020. p. 3895–3900.

82. Albert ST, Shadmehr R. Estimating properties of fast and slow adaptive processes during sensorimotor adaptation. Journal of Neurophysiology. 2018;119:1367–1393.

83. Avraham G, Keizman M, Shmuelof L. Environmental consistency modulation of error sensitivity during motor adaptation is explicitly controlled. Journal of Neurophysiology. 2020;123:57–69.

84. Davison EJ. The robust control of a servomechanism problem for linear time-invariant multivariable systems. IEEE Transaction on Automatic Control. 1976;21(1):25–35.

85. Broucke ME. Adaptive internal model theory of the oculomotor system and the cerebellum. IEEE Transactions on Automatic Control. 2021;66:5444–5450.

86. Broucke ME. Adaptive Internal Models in Neuroscience. Foundations and Trends in Systems and Control. 2022;9(4):365–550.

87. Herzfeld D, Vaswani P, Marko M, Shadmehr R. A memory of errors in sensorimotor learning. Science. 2014;345:1349 –1353.

88. Wang T, Ivry R. A cerebellar population coding model for sensorimotor learning. bioRxiv. 2024;doi:10.1101/2023.07.04.547720.

89. Donchin O, Rabe K, Diedrichsen J, Lally N, Schoch B, Gizewski E, et al. Cerebellar regions involved in adaptation to force field and visuomotor perturbation. J Neurophysiology. 2012;107:134–147.

90. Apps R, Garwicz M. Anatomical and physiological foundations of cerebellar information processing. Nature Review Neuroscience. 2005;6(4):297–311.

91. Gao Z, Proietti-Onori M, Lin Z, Brinke MT, Boele H, et al JP. Excitatory cerebellar nucleocortical circuit provides internal amplification during associative conditioning. Neuron. 2016;89:645–57.

92. Houck B, Person A. Cerebellar loops: a review of the nucleocortical pathway. Cerebellum. 2014;13:378–385.

93. Houck B, Person A. Cerebellar premotor output neurons collateralize to innervate the cerebellar cortex. Journal of Comparative Neurology. 2015;523(15):2254–2271.

94. Andersson G, Garwicz M, Hesslow G. Evidence for a GABA-mediated cerebellar inhibition of the inferior olive in the cat. Experimental Brain Research. 1988;72:450–456.

95. Kenyon G, Medina J, Mauk M. A mathematical model of the cerebellar-olivary system I: self-regulating equilibrium of climbing fiber activity. Journal of Computational Neuroscience. 1998;5:17–33.

96. Rasmussen A. Graded error signals in eyeblink conditioning. Neurobiology of Learning and Memory. 2020;170:107023.

97. Rowan M, Bonnan A, Zhang K, Amat S, Kikuchi C, Taniguchi H, et al. Graded control of climbing-fiber-mediated plasticity and learning by inhibition in the cerebellum. Neuron. 2018;99:999–1015.

98. Yang Y, Lisberger S. Purkinje-cell plasticity and cerebellar motor learning are graded by complex-spike duration. Nature. 2014;510:529–532.

99. Lisberger S. Neural basis for motor learning in the vestibuloocular reflex of primates. III. Computational and behavioral analysis of the sites of learning. Journal of Neurophysiology. 1994;72(2):974–998.

100. Dum R, Strick P. An unfolded map of the cerebellar dentate nucleus and its projections to the cerebral cortex. J Neurophysiology. 2003;89:634–639.

101. Bostan A, Dum R, Strick P. Cerebellar networks with the cerebral cortex and basal ganglia. Trends Cogn Sci. 2013;17(5):241–254.

Behavior	Experiment	F	F_n	$\psi_\circ$	A_f	A_{fn}	b_f	L_f
Classical Behaviors	Savings with CP	0.9	$*$	1	$*$	$*$	$*$	$*$
	Spontaneous Recovery	0.9	$*$	1	$*$	$*$	$*$	$*$
	Evoked Recovery	0.9	$*$	1	$*$	0.95	0.05	$*$
	Bansal, 2023	0.7	$*$	0.9	0.9	0.95	0.05	$*$
	Bond & Taylor, 2015	0.7	$*$	1	$*$	0.95	0.05	$*$
Error Clamp	Morehead, 2017	0.7	$*$	$*$	0.9	0.95	0.05	$*$
	Kim, 2018	0.7	$*$	$*$	0.9	0.95	0.05	$*$
	Tsay, 2021	0.7	$*$	$*$	0.95	0.95	0.1	0.005
	Ignore-N (CW)	0.7	$*$	1	0	0.95	0.05	0.005
	Ignore-N (CCW)	0.7	$*$	0.8	0	0.95	0.05	0.005
	Learn-N (CW)	0.7	$*$	1	0	0.95	0.05	0.005
	Learn-N (CCW)	0.7	$*$	0.8	0	0.95	0.05	0.005
	Ignore-W	0.7	$*$	0.9	0	$*$	0.01	0.002
	Learn-W	0.7	$*$	0.9	0	$*$	0.01	0.002
Savings	Avraham, 2021	0.9	0.92	0.9	0.9	0.95	0.05	$*$
	Fig 2A, Yin, 2020	0.85	0.95	0.9	0.6	0.92	0.02	$*$
	Fig 2B, Yin, 2020	0.85	0.9	0.9	0.6	0.92	0.05	$*$
Phase Switch	Ruttle, 2021	0.7	$*$	1	0	0.8	0.01	0.005
	Amario, 2024	0.7	$*$	1	0	0.9	0.01	0.005

Table 2. Model parameters for simulations. Entries with a * indicate the parameter plays no role in the behavior.